EXPERIMENTS INVOLVING SECOND ORDER EFFECTS IN HIGH-INTENSITY, HIGH-FREQUENCY ACOUSTIC FIELDS

by

KEVIN MICHAEL WANKLYN

B.S., Kansas State University, 2000
M.S., Kansas State University, 2002

AN ABSTRACT OF A DISSERTATION

submitted in partial fulfillment of the requirements for the degree

DOCTOR OF PHILOSOPHY

Department of Mechanical Engineering
College of Engineering

KANSAS STATE UNIVERSITY
Manhattan, Kansas

2008

Abstract

Cavitation is a long studied phenomenon, fascinating and varied. Observed cavitation thresholds vary, typically ranging from the vapor pressure of the liquid to several atmospheres. Recent studies in cavitation involving very clean liquids give rise to thresholds that surpass 100 atmospheres. Calibrating such high intensity, high frequency, focused acoustic fields presents a significant challenge. The present investigation describes how it is possible to exploit the second order acoustic effect of radiation pressure to seek reliable calibration of the high intensity acoustic fields. Experiments describe how to account for the attendant second order effect of acoustic streaming in the evaluation of the radiation force to accomplish meaningful calibration. Beyond the measurement of the second order quantities associated with cavitation, the work also presents a first investigation of a direct estimation of implosion energies of collapsing bubbles near well-characterized surfaces.

EXPERIMENTS INVOLVING SECOND ORDER EFFECTS IN HIGH-INTENSITY, HIGH-FREQUENCY ACOUSTIC FIELDS

by

KEVIN MICHAEL WANKLYN

B.S., Kansas State University, 2000
M.S., Kansas State University, 2002

A DISSERTATION

submitted in partial fulfillment of the requirements for the degree

DOCTOR OF PHILOSOPHY

Department of Mechanical Engineering
College of Engineering

KANSAS STATE UNIVERSITY
Manhattan, Kansas

2008

Approved by:

Major Professor
Sameer I. Madanshetty

Copyright

Abstract

Cavitation is a long studied phenomenon, fascinating and varied. Observed cavitation thresholds vary, typically ranging from the vapor pressure of the liquid to several atmospheres. Recent studies in cavitation involving very clean liquids give rise to thresholds that surpass 100 atmospheres. Calibrating such high intensity, high frequency, focused acoustic fields presents a significant challenge. The present investigation describes how it is possible to exploit the second order acoustic effect of radiation pressure to seek reliable calibration of the high intensity acoustic fields. Experiments describe how to account for the attendant second order effect of acoustic streaming in the evaluation of the radiation force to accomplish meaningful calibration. Beyond the measurement of the second order quantities associated with cavitation, the work also presents a first investigation of a direct estimation of implosion energies of collapsing bubbles near well-characterized surfaces.

Table of Contents

List of Figures

List of Tables

Nomenclature

α	absorption coefficient
θ	angle
$^\circ$	degree
λ	wavelength
μ	dynamic viscosity
μm	micron
μN	micronewton
ρ	density
σ	surface tension
A	area
AC	alternating current
AFM	Atomic Force Microscope
AIUM	American Institute of Ultrasound in Medicine
atm	atmosphere
c	speed of sound
cc	cubic centimeter
dB	Decibel
CCD	charge coupled device
cm	centimeter
DF	duty factor
ENI	Electronic Navigation Industries
F	force
f	frequency
F_d	drag force
F_{rad}	radiation force
g	acceleration due to gravity
gm	gram
Hz	Hertz
i	electrical current
in	inches
I	acoustic intensity
K	Kelvin
k	wave number
K_{ssp}	calibration constant of SSP
K_{trans}	calibration constant of transducer
K_{lobe}	calibration constant of acoustic lobe
kg	kilogram
kHz	kilohertz
l	suspension length
LDV	Laser Doppler Velocimetry
M	geometric factor
m	meter
m_t	mass of target
mm	millimeter
ml	milliliter
MΩ	megaohm
MPa	megapascal
ms	millisecond
NEMA	National Electrical Manufacturers Association
nm	nanometer
OD	optical density
P	pressure
P_0	static pressure

p	peak pressure amplitude
p_g	pressure of gas inside bubble
PAL	Physical Acoustics Laboratory
PC	personal computer
PIV	Particle Imaging Velocimetry
pm	picometer
ppm	parts per million
PRF	pulse repetition frequency
PW	pulse width
PVDF	polyvinylidene difluoride
PZT	lead zirconate titanate
RC	reflection coefficient
R_e	resistance
R	bubble radius
r	radius
RP	Rayleigh-Plesset
s	second
SNAP	System for Non-linear Acoustic Phenomena
SSP	sound signal at a point
T	transmittance
T_s	tension
TC	transmission coefficient
t	time
U	velocity of a wave
UPW	ultra pure water
UV	ultraviolet
V	voltage
v	velocity
$\bar{V}$	time average of voltage
$\forbar{V}$	volume
V_{p-}	volts peak negative
V_{ssp}	voltage measured by SSP
W	watt
$\dot{W}$	acoustic power
x	multiplier
Z	acoustic impendence

Acknowledgements

It has been my experience that there are numerous people who aid in the education of an individual student. The people who have assisted me are numerous and each deserves recognition and acknowledgement. Their assistance, guidance, and advice have been something that I truly appreciate.

It sometimes goes without saying, but an important part of my education has been my fellow students. Whether they sat beside me as classmates, or I stood in front of them as an instructor, their perspectives have been enlightening. Some have helped me work through a graduate school project and others have asked me interesting questions in an undergraduate course. It has shown me that there is often more than one perspective and usually more than one journey to a solution.

There are four individuals whom I hold in very high regard. The first is Dr. Sameer Madanshetty, my major professor. I greatly appreciate his patience and knowledge. Two others I have watched go through this process before me. Each I have learned from, each has taken the time to make sure I understand. The unwavering friendship and wisdom of Dr. Hang Ji and Dr. Bingrong He is worthy of note. Additionally, David Hill is a machinist and educator, who always seems to find the cleverest way to build one of my designs and along the way show immense kindness, patience, and care as he passed on knowledge that he has learned in his impressive career. I would also like to thank the people of Uncopiers, Inc., Manhattan, Kansas for their support both financially and with their facilities.

The group of people who deserves the most acknowledgement, however, is my family. I have a younger brother named Craig who continues to impress me with his dedication and stubbornness. I have a father and mother whom I would not trade for anything. I get up every day to make these people proud. In turn, they are always there to act as a proofreader, a problem solver, or a friendly ear. They are my support team. I am glad I was drafted by them 29 years ago.

Dedication

To my alma mater
Faithful to its colors, I shall ever be.

Chapter 1 - Introduction

This dissertation experimentally investigates aspects of high-intensity, high-frequency ultrasound, particularly in pulsed and focused fields occurring in water. The particular areas of interest are calibration of acoustic fields, the second order acoustic effects of radiation force and streaming, and estimation of energy deposition of an acoustically produced cavitation bubble. These four areas, when separated, could provide a wealth of research both theoretical and experimental. Together, their study creates a better understanding of the effects of focused, pulsed ultrasonic fields.

Research in acoustics (as well as all other scientific pursuits) requires following a standard system of procedures and guidelines to conclude concrete results. This research will follow three "golden rules" proposed by Apfel (1972). Dr. Apfel was a renowned researcher in the field of acoustics and acoustically produced cavitation. His papers presented the seminal studies in the subject. His rules when dealing with the study of acoustics and its related effects are: 1) Know thy liquid, 2) Know thy sound field, and 3) Know when something happens. The use of these three rules will introduce the research described in this dissertation. The descriptions provided in this introduction are consistent in all aspects of this investigation into high-intensity, high-frequency ultrasound. Any deviation will be specifically mentioned.

1.1 A second order effect

This research will take advantage of two second order effects of high-intensity acoustic fields in a water medium. What is a second order effect? A straightforward way to explain this is by using an electrical analogy to the studied acoustic system that most should be familiar: current passing through a resistor.

If an alternating current (AC) passes through a resistor, the time average of the voltage is found by integrating the product of the current and the voltage over a set number of periods of the signal.

$$\bar{V} = \int_0^{2\pi} R_e i \sin\theta \, d\theta \qquad \textbf{(1.1)}$$

Since the resistance is constant, the result of this integral is zero since the integral of a sine function over a period is zero. However, if instead of having a constant resistance the resistance varied with the current, the integral would have a $\sin^2$ term, and the resulting integral would produce a constant value.

$$\bar{V} = \int_0^{2\pi} R_e i \sin^2 \theta \, d\theta \qquad \textbf{(1.2)}$$

The change of the resistance based upon the AC current driving the system is a second order effect. In our acoustic situation, the acoustic waveform is a longitudinal wave passing through a water medium. In response to this waveform, the properties of water will change slightly like the resistance in the analogy producing a small, constant, measurable effect. Experimentally to observe the properties of high-intensity acoustics, this research will take advantage of these second order effects.

1.2 Know thy liquid

This research applies the use of high-intensity ultrasound in water. In order to have consistent, repeatable results, this water must be of controlled quality. A custom-made Ultra-Pure Water (UPW) system was created for this purpose. This system can consistently produce water that fits into the qualifications the research requires. Feed water entering the system encounters many levels of purification before it comes to the point of use (carbon filtration, course prefiltering, reverse osmosis, deionization, UV lamp irradiation, and optional degassing concluded by flowing through a series of final filters ending in the desired filtration rating). This water has a high resistivity[1] of 15 MΩ cm or higher. If the context of the experimentation requires it, this water system creates water of different ionic purities, dissolved gas contents, and final filtration values. The pore size of the final filter in series defines the UPW in this research. Currently the system can produce three levels of filtration: 0.2 micron, 0.1 micron, and 0.05 micron. Filters of decreasing pore size placed in series create the desired filtered purity of water.

[1] The resistivity is a function of mixed bed deionizing resin that interacts with the water, removing the ionic content. Over time, ionized water consumes the resin, lowering the level of resistivity. When newly installed, the water resistivity is as high as 18 MΩ cm, but over time, it slowly decreases. Typically, replacement occurs once this level lowers to 15 MΩ cm.

It is important to note that the rating of filter membranes is not a trivial task. Typically, there are two ways to rate filters. The first method involves challenging a filter with particles and using an optical method to count and size particles not retained by the filter. This technology is presently limited to sizing filters down to 50 nm. Below this point, a bubble point test is used which involves wetting a filter and then pressurizing it with air to determine when bubble breakthrough occurs. This method does not produce absolute answers. Thus, ratings of a specific filter can vary from manufacturer to manufacturer. One must pay attention to not only the rating of a filter, but also the method of determining that rating and the confidence level of the retention of particles at the filter. In short, not all 0.2 micron filters act alike (Williamson, 2008).

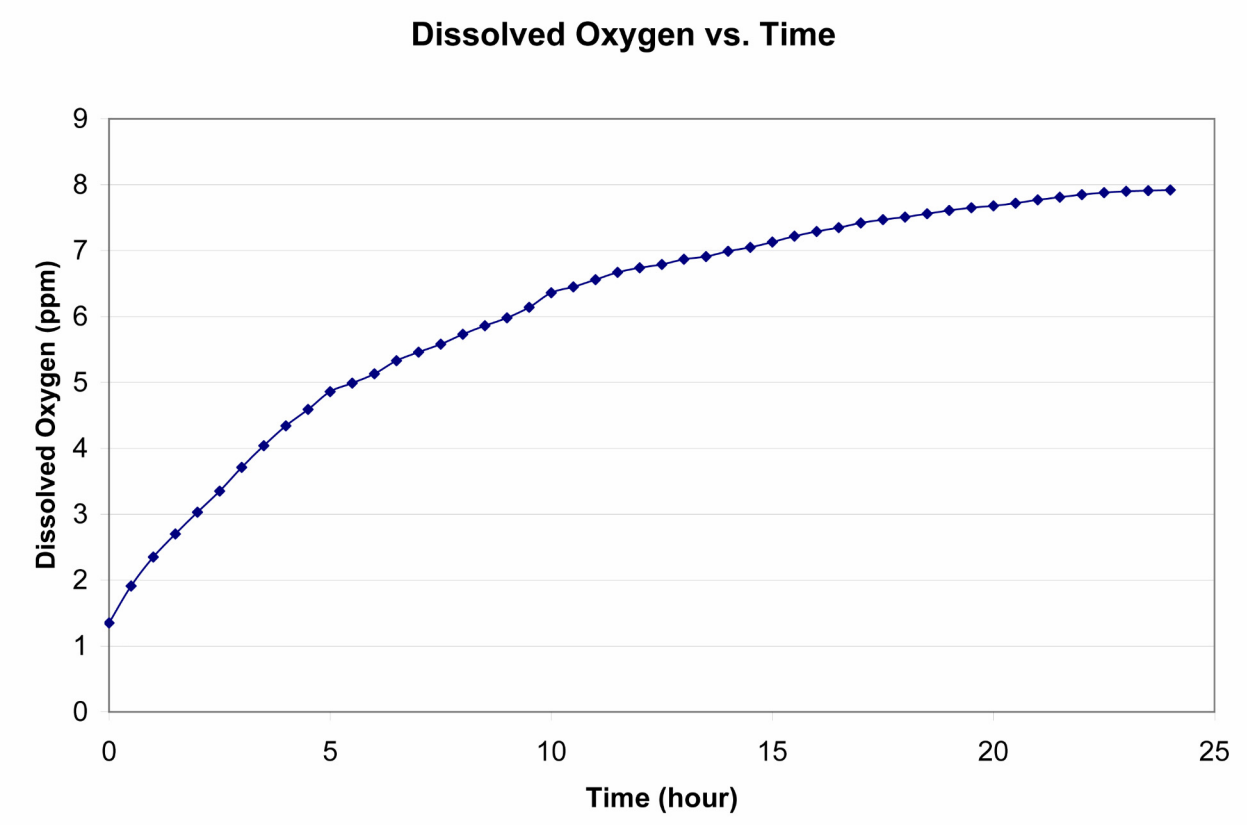

Figure 1-1: Dissolved oxygen content vs. time (adapted with permission from He (2004))

Besides filtration, a researcher may degas the final water sample by independently controlling the degassing membranes present in the system. An Orion model dissolved oxygen meter found that water which has not been degassed had a value of approximately eight parts of oxygen per million (ppm) while degassed water could be created (when conditions were right) to

have a reading as low as 0.5 ppm. Dissolved oxygen content is of particular importance when studying acoustically created cavitation, as there may be a relationship between the occurrence of cavitation and the level of dissolved oxygen. Figure 1-1 shows the dissolved oxygen readings of a particular sample of water. This water was collected from the water system filtered to 0.2 micron, placed in a 1000 ml glass beaker, and allowed to sit in a laboratory environment. Regular measurements with an Orion dissolved oxygen probe showed that over time, a sample of water degassed to 1.3 ppm would slowly increase in oxygen content.

The desire of this research is to investigate the second order effects of high intensity acoustics alone and "ignore" the water as being constant. This required following strict guidelines in water preparation. Although with time and interaction with the atmosphere minor changes in dissolved oxygen content and resistivity occurred, repeated experimentation observed that well monitored water quality produced a negligible effect on acoustic experimentation.

1.3 Know thy sound field

In the research presented in this dissertation, the first element necessary to produce a proper acoustic field is a reliable water source. The description and preparation of the water by the UPW system as described in Section 1.2 assures this fact. What follows is a description of the elements used to create the sound field the transducer and the amplification system.

1.3.1 The transducer

The definition of a transducer is an object that receives energy in one form and converts it to another form. In this research, the transducer is a submergible, megasonic, piezoelectric crystal mounted in an appropriate housing that turns an electrical wave into a pressure wave and vice versa. The acoustic transducer used in this study is a custom-made unit using a PZT (lead zirconate titanate) crystal. The acoustic energy of the transducer is concentrated by machining the crystal so that its focus is at a point. PZT transducer elements have been poled so that they have a positive and negative face. A conductive material covers these faces. A stainless steel housing holds the completely manufactured crystal and a very thin layer of Teflon covers the water facing surface. A UHF connector is available at the back of the housing to allow connection to an amplification system.

The properties of a transducer's acoustic field must be measured and the sensitivity known in order to use it successfully. This is why calibration is such an important step before

placing a transducer in service. Complete calibration of a transducer not only involves finding its driving voltage input / pressure output relationship, but also finding other aspects of the acoustic field such as its resonance frequency, focal distance and various types of beam profiles. Often, calibration requires the use of a reference hydrophone. Chapter 2 further discusses the topic of calibration since the transducer is a cornerstone in this research.

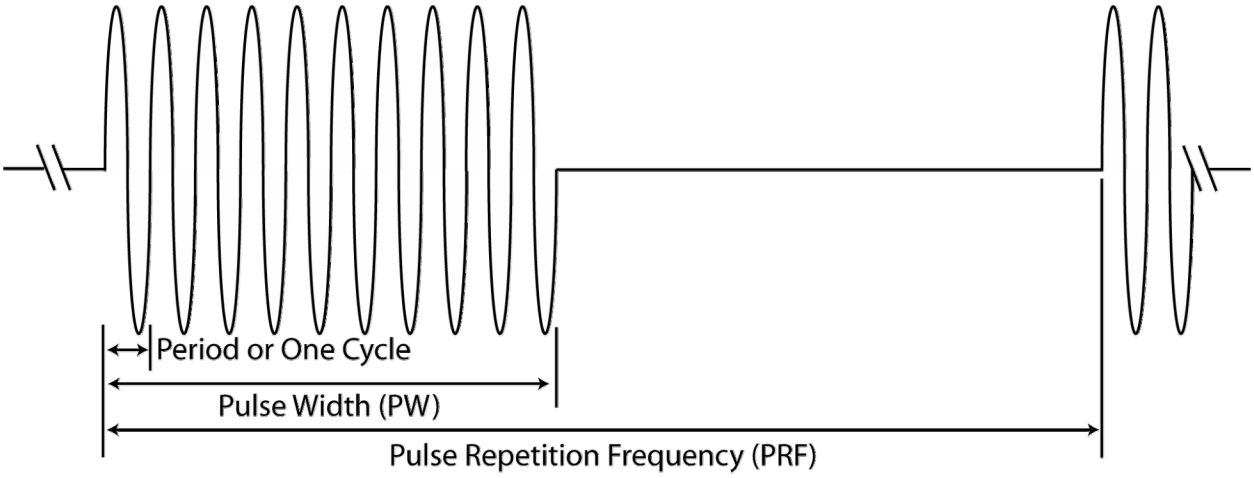

Figure 1-2: An illustration of the variables in duty factor creation

In the research described in this dissertation, a continuous wave did not drive the transducer. Most commonly, very low duty factors (between 0.1% and 5%) drove the transducer. Figure 1-2 shows an illustration of the variables in pulsed acoustics. There are many ways to create a specific duty factor by varying the pulse width (PW) and pulse repetition frequency (PRF) appropriately with respect to one another. This study will take advantage of this fact.

Low duty factors also allow for interesting uses of the transducer. In this research, the greatest duty factor used is 5 %. This means that the transducer is outputting a signal 5 % of the time and off (or "silent") 95 % of the time. (In many situations, the duty factor is 0.1 % leading to an off time of 99.9 %.) The use of acoustics at low duty factors allows the transducer to act as a receiver during the time in which it does not produce an acoustic signal. Due to the piezoelectric nature of the transducer's crystal, any acoustic signal received by the transducer during the silent time is converted to an electrical waveform. Computerized analysis of this received and converted signal generates valuable acoustic information from the water medium. Because of this, a single transducer can at times take the place of a configuration of multiple transducers and provide additional benefits of being a self-contained pulser-receiver.

1.3.2 The amplification system

There are two different types of driving amplifiers used in this research. One was a traditional amplifier that required an input driving signal provided by a function generator. In this situation, the amplifier was an Electronic Navigation Industries (ENI) A-300. An Agilent 33250A function generator created the input waveform. A LeCroy LA354 oscilloscope verified the waveform created. The ENI A-300 / Agilent 33250A system provided a wide range of duty factors and driving modes.

Another powerful type of amplifier used in this research was a SNAP (System for Non-linear Acoustic Phenomena). The SNAP combined waveform generation, amplification, and analysis in one unit. This system had a built-in PC card connected to and controlled by terminal software on a computer. This custom-made system provided the user with additional functions and analysis options that a traditional stand-alone amplifier could not provide. The SNAP could send a driving signal while analyzing a returned received signal. This allowed for real time signal monitoring and analysis. Another benefit of the SNAP was that it was PC-controlled with Windows-based software. This allowed for convenient data storage. Contrary to these advantages, the SNAP had a limited range of power output that it could create. In situations requiring higher power output, the ENI A-300 / Agilent 33250A system replaced the SNAP.

1.4 Know when something happens

This dissertation investigates the effects of high-intensity ultrasound. Therefore, the goal of this study is to "know when something happens." One effect of high-intensity ultrasound that occurs quite frequently is cavitation. Cavitation is defined as the formation and collapse of bubbles in liquids (Leighton, 1994). The word "formation" describes the creation of new bubbles (voids, cavities) in a host medium or the expansion of pre-existing ones. When these newly formed bubbles collapse (or implode), they produce tremendous energy densities. This energy deposition can cause erosion of even the most advanced material, sonoluminescence (acoustically produced light), an increase in the performance of chemical reactions, as well as many other phenomena.

Even though the formal study of cavitation is over 110 years old (and even then, some researchers were close to its discovery farther back), there are still many questions to be

answered and concepts to be studied. Note that the study of cavitation has a non-acoustic origin, but has very strong ties to the study of high intensity sound fields.

1.4.1 The history of cavitation

Humans' desire to move quickly led to the discovery of cavitation. As early as 1873, Osborne Reynolds (of Reynolds Number fame) began to study the phenomenon that caused the racing of engines in screw steamer ships (Jackson, 1995). Although nowhere in his papers does he use the word "cavitation," today we recognize that what he was describing is the phenomenon of cavitation.

The initial testing and speed trial of the first modern naval destroyer is the first recorded use of the word "cavitation." During testing of the British ship H.M.S. Daring in 1894, bubble formation, severe vibration, and surface damage to the propellers were reported (Suslick, 1990). At the time, Froude coined the name "cavitation" to describe the occurrence. After that test the UK Admiralty charged Lord Rayleigh to investigate the phenomenon (Thornycroft & Barnaby, 1895). He later produced the first mathematical model for the collapse of cavities in incompressible liquids in his paper, "On the pressure developed in liquid during the collapse of a spherical cavity." All understood at the time was that these cavitation bubbles had the ability to concentrate and deposit large amounts of energy on to surfaces. Predictions were made that through cavitation, local temperatures of 10,000 K and pressures of 10,000 atm could be produced in the collapse (Suslick, 1990).

At this point or soon thereafter, a fracture in the study of cavitation most likely occurred. One group of scientists and engineers concentrated on finding a way to limit the damaging effects of cavitation through design and procedural methods. Another group saw the enormous potential in these collapsing bubbles and chose to search for a way to harness the energy that cavitation provides to help solve unique engineering problems. Looking at both approaches it is clear that cavitation has an interesting reputation both positive and negative. Designers of pumps, for example, consider cavitation a detriment. Conversely, other completed studies (such as those in cleaning of microelectronics) propose that cavitation is a subject full of potential to solve novel engineering problems.

1.4.2 What is cavitation?

The phase diagram of water shows that a phase change from liquid to gas can occur through two different methods: 1) an increase in temperature, and 2) a decrease in pressure. Figure 1-3 shows the phase diagram of water. This figure presents two direct paths from liquid water to water vapor. If choosing path one (a line of increasing temperature), the phenomenon is referred to as boiling. In path two, the local static pressure of the liquid falls below its vapor pressure changing liquid to vapor in a process referred to as cavitation. Focusing on the phase change of the liquid, cavitation and boiling produce the same vaporous outcome, thus, in some circles "room temperature boiling" is another name for cavitation.

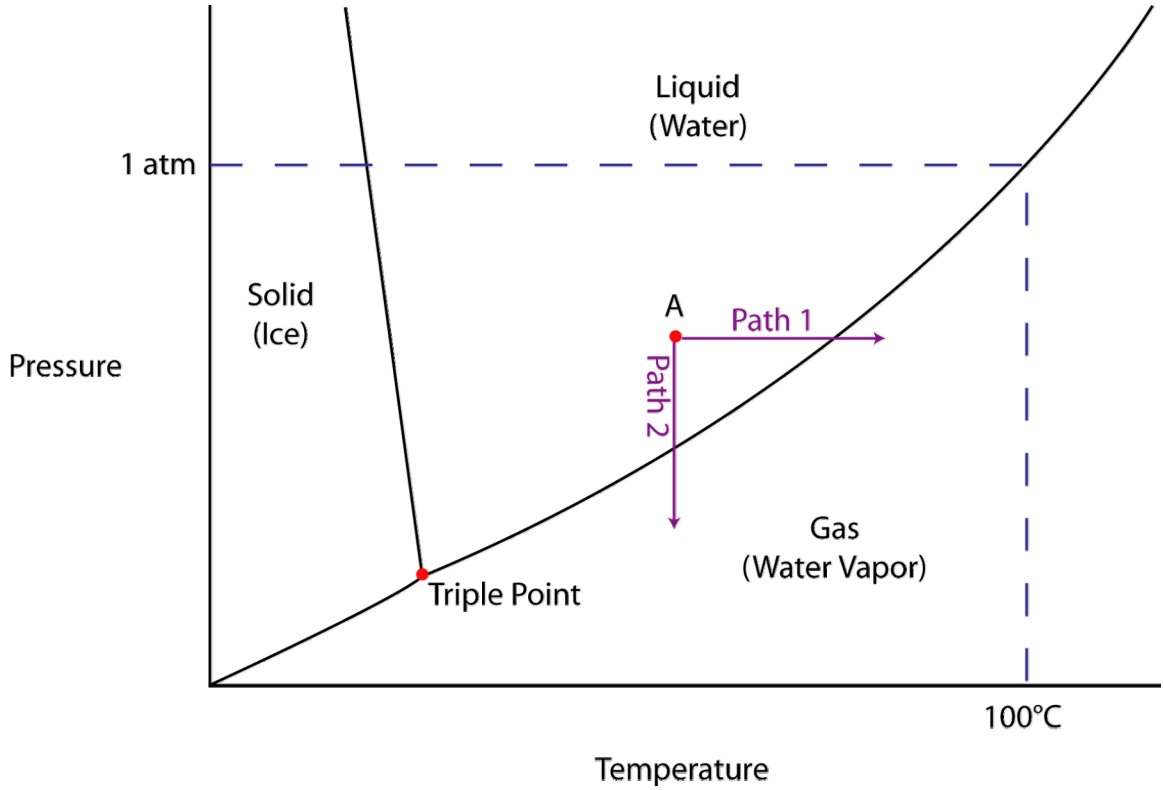

Figure 1-3: The phase diagram of water showing paths to the vapor phase.

Although the formal definition of cavitation is one that considers a pressure drop below the vapor pressure, a more complete description is provided by Leighton (1994) when he states that cavitation is "the creation of new surfaces or the *expansion / contraction / distortion* of *pre-existing* ones within the body of a liquid." Leighton's definition recognizes the fact that cavitation in a liquid is closely tied to the pre-existing motes that are present in the body of the fluid, and not just the liquid itself.

1.4.3 Types of cavitation

As described before, the mechanism of cavitation is a pressure drop. This pressure drop can occur through many different situations. One cause is rapid velocity changes in fluid flows, often due to a sudden change in geometry. This type of cavitation is hydrodynamic cavitation.

There are different ways to describe hydrodynamic cavitation. "Traveling" cavitation describes a bubble that moves with the flow of the host medium, expanding and contracting along the way. Additionally, cavitation can be called "fixed" if it forms and attaches to a surface or a steady location and remains there in an unsteady state (much like cavitation formed when water at high velocity flows over a notch in a hydrofoil). Figure 1-4 illustrates this type of cavitation. Finally, "vortex," or "tip," cavitation occurs at a region of high shear such as on the edge of a ship's propeller.

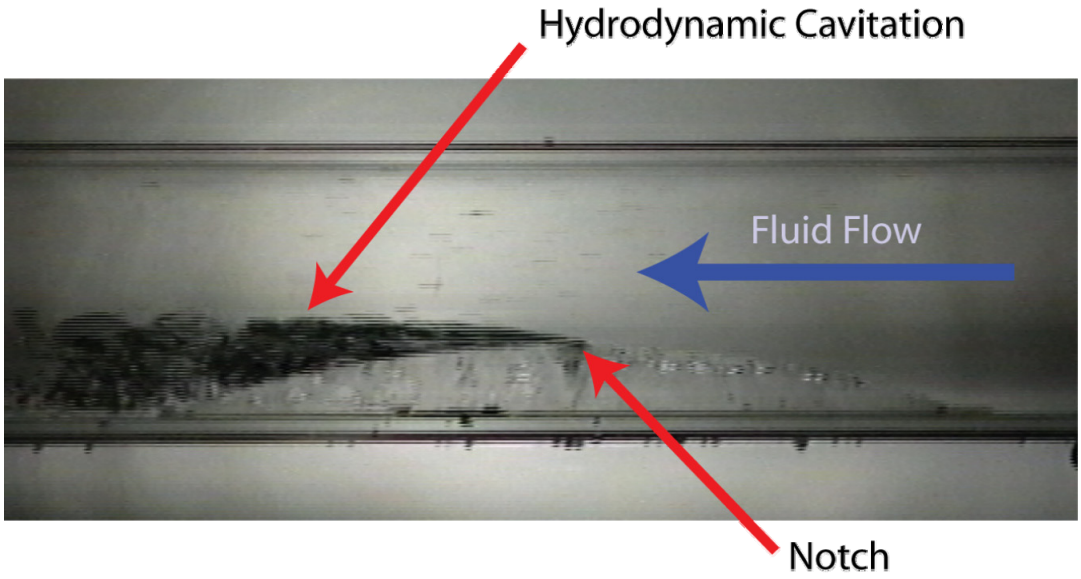

Figure 1-4: Hydrodynamic cavitation caused by flowing water over a notch

In static fluid applications on the other hand, underwater explosions or acoustic methods produce cavitation. All of these areas of study are quite rich in their breadth. This dissertation presents cavitation created acoustically. Acoustic cavitation commonly nucleates through small pre-existing bubbles or in partially wetted motes such as those in the side of a container or on an impurity in the water. The acoustic wave will energize these pre-existing bubbles or unwetted motes to produce cavitation. Shown in Figure 1-5 is the reaction of a bubble from the acoustic wave's tensile and compressive sections. Note the figure presents the waveform as a transverse wave for illustrative purposes only; sound occurs in longitudinal waves.

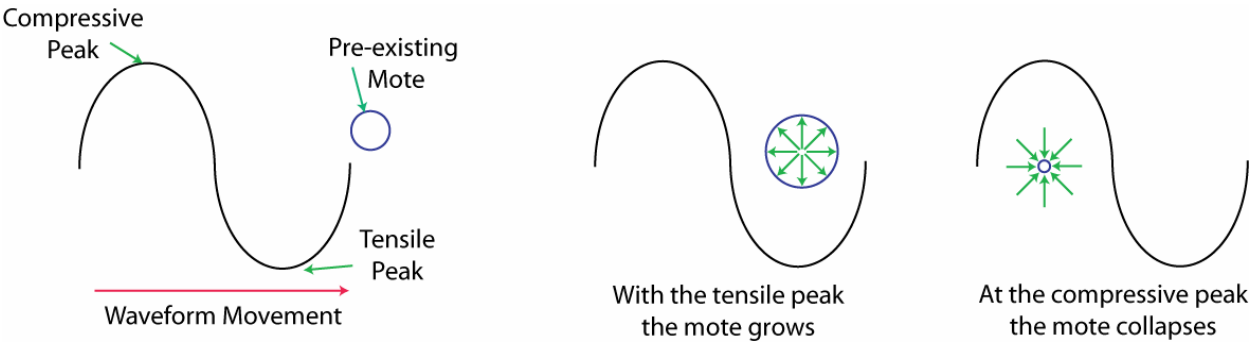

Figure 1-5: Response of a cavity to the tensile and compressive peaks of an acoustic wave.

There are different ways to describe acoustic cavitation as well: steady state and transient. A situation where the cavity or bubble created is "stable" and oscillates about an equilibrium size for many periods of the sound field describes steady state cavitation. This steady-state cavitation bubble would look like it is pulsing, never fully collapsing, always present. Conversely, transient cavitation events have a very short lifetime. These cavitation events expand and implode in a very short time scale.

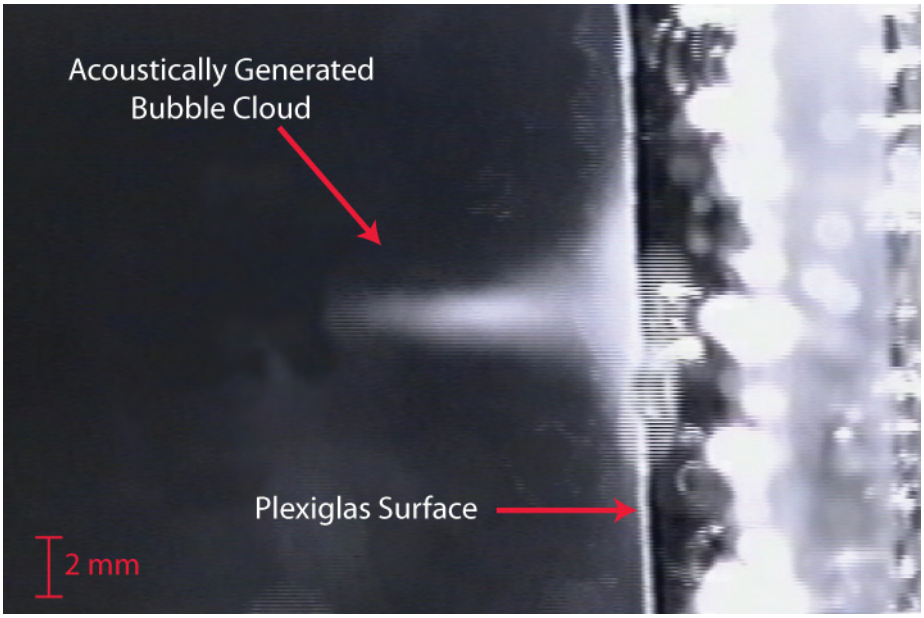

Figure 1-6: Video capture of an acoustically generated bubble cloud near a surface

Additionally, there must be differentiation between single bubble cavitation and cloud cavitation. Single bubble cavitation concerns the growth and collapse of one bubble. Cloud cavitation describes the growth and collapse of multiple bubbles in a region. In cloud cavitation, triggering one cavitation bubble to implosively collapse can cause a chain reaction in the rest of the cloud. An acoustic bubble plume, as seen above in Figure 1-6, is a type of cloud cavitation.

1.4.4 Cavitation thresholds

Since the onset of cavitation is significant in high-intensity, high-frequency fields, a researcher must be aware of the inception point of cavitation. Knowledge of this cavitation threshold allows for the control or avoidance of its effects. The determination of the level at which the onset of cavitation occurs characterizes cavitation threshold research. This area of research has inspired many approaches and many different experimental results. There are theoretical values and experimental values; at times even similar methods will provide contradictory results. There is no conclusive answer as to what is the definitive value for the cavitation threshold of a water sample.

Previous research using high-intensity, focused, pulsed ultrasound resulted in data describing consistent and repeatable threshold values (Wanklyn, 2006). This experimentation provided valuable information showing under what conditions cavitation produced by such ultrasound would occur. This data will be of specific interest in every aspect of the research completed for this dissertation.

1.5 The scope of this study

The purpose of the work in this study is to investigate further the effects of pulsed, high-intensity ultrasound. The author has studied many interesting applications of this type of ultrasound, including: removing thin films from their substrates precisely, cleaning particles off of very fragile substrates, measuring adhesion strengths of thin films, and determining the acoustic cavitation threshold of water. On the surface, these areas of research may seem like different focuses in the study of high-intensity, pulsed ultrasound and its effects; however, they each rely on common principles.

The motivation for this research initiated with the study of cavitation thresholds – the search for the first pressure at which cavitation will occur in a liquid. A common liquid for study is water, however; water samples are not standardized. This is a major problem leading to large variation in measured cavitation thresholds. Typically, the cavitation threshold for water is the vapor pressure of water or one or two atmospheres peak negative. Thresholds of these water sources can be measured using commonly available acoustic transducers. Present filtration technology allows common water sources to be highly purified creating a specialized UPW quality source. Thresholds of this water exceed 100 atmospheres. The use of commonly

available transducers is not possible when investigating this water acoustically. Threshold determination of this finely filtered water requires acoustic sources of higher intensities. This necessitates the need for calibration of transducers that produce these high-intensity fields. Note that high-intensity, high-frequency fields pose significant challenges not experienced in relatively low-intensity fields.

Calibration of high-intensity fields is the cornerstone of all research into the subject. One must understand what output an acoustic transducer is providing to be able to analyze intelligently the results. In this research, the intensities used produce pressures that exceed those values directly measured and verified using standard reference hydrophones because of the occurrence of cavitation. Cavitation created by these intensities will damage a reference hydrophone and render it useless. This requires the proposal of another technique that will verify the calibration constant over the range of operation of the transducer. An absolute calibration method using the second order acoustic effect of radiation force will allow the calibration constant of a transducer to be experimentally verified. Radiation force is a subtle effect of a high intensity acoustic field. In fact, an acoustic pressure of 10 MPa can produce a radiation force of approximately 1 dyne. This illustrates the fact that radiation force measurements are extremely delicate and require enormous patience and practice. Chapter 2 will investigate this topic.

When taking advantage of radiation force to calibrate high-intensity fields, the associated second order effect of acoustic streaming (flow caused by acoustic means) will become relevant. When measuring radiation force using a delicate force balance target at high intensities, a purely reflecting target may measure deflection caused by not only radiation force, but also by acoustic streaming. To get accurate radiation force measurements one must subtract the streaming deflection from the overall deflection. Chapter 3 experimentally investigates streaming caused by high-intensity fields.

Another phenomenon that affects the radiation force target is sustained “cloudlike” cavitation that occurs at very high intensities. This cavitation will cause the target to “flutter” and make it difficult to measure accurately radiation force or the associated streaming. Single cavitation events will not affect the measurement. This leads one to be interested in finding if the energy of a single cavitation event can be determined or estimated. This dissertation will describe a method to estimate this energy by exposing the well-characterized, single crystalline surface of a silicon wafer to pit producing cavitation. The result will be recognizable pitting on

this surface traceable to a single cavitation event. Measurement of the energy needed to create such pitting will estimate the mechanical energy of cavitation. Chapter 4 will describe the apparatus and procedure necessary for this estimation.

Chapter 2 - Calibration of High-Intensity Acoustic Fields

Calibration is the cornerstone of the study of high-intensity acoustic fields. With acoustic fields created by piezoelectric transducers, knowing only the input electrical power and the insonification time does not help in determining the details of an acoustic event. A meaningful analysis requires the knowledge of pressure output. Without proper calibration, this pressure / voltage relationship is unknown to the researcher. This chapter will be devoted to looking at the calibration methods and systems needed for high-intensity ultrasound. In particular, the idea of calibration using acoustic radiation force will be established and examined.

2.1 Reference hydrophones

Calibration of acoustic transducers is a delicate operation. The reason is that acoustically produced cavitation (many times the exact phenomenon that high-intensity ultrasound is used to produce) can be the very thing that derails calibration. In many cases, in order to determine the pressure that a transducer is producing to create a calibration curve, a reference hydrophone is used. These reference hydrophones arrive pre-calibrated from the manufacturer. Many of the commercially available reference hydrophones use sensitive Polyvinylidene Difluoride (PVDF) membranes. PVDF exhibits piezoelectricity several times larger than quartz. Unlike in ceramics, where the crystal structure of the material creates the piezoelectric effect, in polymers the intertwined long-chain molecules attract and repel each other when an electric field is applied (Vinogradov & Schwarz, 2002).

If, when using a PVDF hydrophone, the acoustic transducer produces an intensity that will create a cavitation event and that event deposits its energy on the PVDF sensing element of the reference hydrophone, irreversible damage can occur. This illustrates the problem that arises in calibration of acoustic transducers; a direct measure of the calibration constant is not possible at high intensities due to the threat of reference damaging cavitation.

Calibrated reference hydrophones can be quite expensive. Thus, a single cavitation event caused by a single instance of low pressure can be very costly. To ensure that cavitation events do not occur when using such hydrophones, a user must exhibit appropriate care with the delicate devices. Because water quality can lower cavitation thresholds, the creation of the water

medium when using reference hydrophones is of the utmost importance. To raise the cavitation inception point, the water used in this testing should be of UPW testing, and if available, degassed.

2.2 Confronting the calibration "problem"

Elimination of possible damage to reference hydrophones requires careful preparation of the host water and monitoring of the maximum acoustic intensity. However, a problem arises when the output of a transducer needs verification above the cavitation threshold. One of these situations is the calibration of transducers producing high-intensity acoustic fields. A reference hydrophone cannot successfully provide this verification. Direct calibration methodology using reference hydrophones is not practical at such levels.

To approach this problem the development of a new type of hydrophone occurred. This hydrophone was an economical and robust alternative to the expensive and delicate reference hydrophones commercially available. These new hydrophones have been named SSP, for Sound Signal at a Point (Greenway, 1999). Manufacturing of the SSP follows a standardized process and an experienced individual can readily produce a quality device when requested. It is important to note that these SSPs are not inexpensive but they do cost less than commercially available reference hydrophones. It is not the intent for these devices to be "throw away"; however, a researcher can feel more freedom to experiment with them in situations where damage could occur to an expensive and delicate reference hydrophone. It is important to note that an SSP can withstand short bursts of cavitation. A rapid flickering of the SSP voltage trace on an oscilloscope indicates when this occurs. Upon prompt removal or reduction of pressure, the SSP can be used again without any deterioration in quality. Additionally, in some cases recalibration of SSPs subjected to substantial cavitation (which lowers their response sensitivity) allows them still to be used successfully.

These "in-house" manufactured SSPs require calibration, leading to the development of an absolute calibration method. Using this technique, SSPs have been shown to have comparable responses to their commercially available counterparts (Chandran, 2000). Calibration of the SSPs can occur at low intensity acoustics if a reference hydrophone of known calibration is available for direct comparison. Alternatively, a transducer of known calibration constant can be used to find the calibration constant of the SSP. In such a case where a reference

is not available to calibrate an SSP, an absolute calibration technique using radiation force balance can be applied (Madanshetty & Chandran, 2005).

2.3 Radiation force

A progressive ultrasound wave produces a steady force (called the radiation force) directed along the beam in the direction of propagation. In a fluid medium such as water, the water is not able to respond fast enough to the transitions between positive and negative pressures; thus, its motion becomes out of phase with the acoustic wave, and energy deposits into the water. This energy results in momentum transfer in the direction of wave propagation. The momentum transfer generates the second order effect of radiation force. (Trahey, Palmeri, Bentley, & Nightingale, 2004) Radiation force is a constant value and does not vary temporally with the fluctuation of sound pressures. A transducer driven at a given voltage will produce a steady radiation force. This allows for a direct and repeatable measurement.

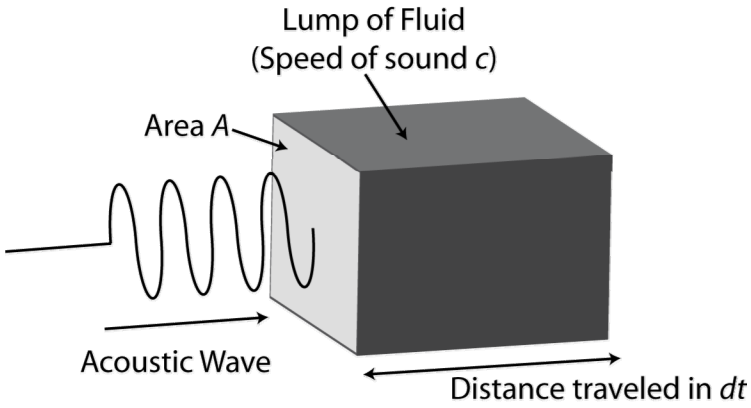

Figure 2-1: A perfectly absorbing fluid lump

Consider an acoustic wave approaching a cube of fluid. (Figure 2-1) This wave has intensity, I (Energy Flux per Area Time) (Leighton, 1994):

$$I = \frac{p^2}{2\rho c} \tag{2.1}$$

Here p is the peak pressure amplitude, ρ the density of the fluid medium, and c the speed of sound in that medium. Assume that the wave incident to the face of the cube crosses it normally and the fluid *completely* absorbs the waveform, the work the wave does on the cube is:

$$Work = I\,A\,dt \tag{2.2}$$

where A represents the area of face of the cube of liquid and dt represents the time needed to absorb fully the waveform.

The cube of liquid in turn does work on the wave in the opposite direction to stop the motion of the wave in the same small change of time:

$$Work = F\,c\,dt \tag{2.3}$$

Equating (2.2) and (2.3) yields a relationship for radiation force for a perfectly absorbing target:

$$F = \frac{I\,A}{c} \tag{2.4}$$

Noting that pressure is force per unit area, the radiation pressure of the incoming wave is:

$$P = \frac{I}{c} \tag{2.5}$$

This situation is assuming a fully absorbing lump of fluid. In the case of a reflecting lump of fluid, the change of momentum is twice as much as the perfectly absorbing case and the pressure is therefore:

$$P = \frac{2I}{c} \tag{2.6}$$

2.4 Experimental measurement of radiation force

Preston (1991) describes several experimental methods by which acoustic radiation force can be measured. A popular method is the calorimetric approach, which measures the rise in temperature when acoustic energy is absorbed and converted directly (and completely) to thermal energy. This technique is difficult because it requires accurate measurement of small temperature increases accurately. Equally popular is a method of using a fully reflecting target and measuring its deflection caused by radiation force. Optical methods use a variation of a Schlieren technique that can prove to be difficult to manipulate and evaluate quantitatively. Proposed electrical methods use a quartz or barium titanate plate that intercepts the acoustic beam after which the charge density is measured. This method has proven to be expensive. Chemical methods often lead to inaccurate results due to exposure times and chemicals involved. Of these methods the most common is either colorimetric or a mechanical technique of the radiation force balance. This research chose the latter of the two.

2.4.1 The radiation force target

In practice, there are two types of radiation force targets used for measurement: absorbing or reflecting. Absorbing targets can create problems because they can increase in temperature creating a target that is not consistent. Because of this, in this research, a reflecting target was be used to determine radiation force. Reflecting targets provide less difficulty to work with as they "perfectly" reflect the acoustic field. However, they too can be problematic when used with continuous waves (as standing waves are created) or when streaming flows are developed that will erroneously add to the deflection of the target. The use of short duty factors in this research avoided the problem of standing waves. This chapter will touch on, and Chapter 3 will further investigate, the phenomenon of acoustic streaming (the bulk movement, or flow, of fluid caused by high-intensity ultrasound) and how it will affect the target.

The reflecting target used does not need to be of any particular size (area); however, it should be of a large enough size to intercept the acoustic wave completely. The only requirement is that it is acoustically reflecting. A mismatch of acoustic impedance, Z, creates a reflecting surface. Analytically, transmission (*TC*) and reflection (*RC*) coefficients for normal incidence show this concept:

$$TC = \frac{2Z_2}{(Z_1 + Z_2)} \tag{2.7}$$

$$RC = \frac{(Z_2 - Z_1)}{(Z_2 + Z_1)} \tag{2.8}$$

If two materials have the same impedance ($Z_1 = Z_2$), then the wave will be completely transmitted (TC= 1, RC = 0), and the fluids are considered impendence matched. Creation of an "acoustic mirror" occurs if the impedances of two materials are substantially different. Air has very low acoustic impedance in comparison to water.[2] Using water as Z_1 and air as Z_2, the reflection coefficient is 0.999 or almost completely reflecting.

[2] acoustic impedance of air = 400 kg/ m² s and water 1.5 x 10^6 kg/ m² s (Leighton, 1994)

2.4.2 Radiation force balance

Figure 2-2 provides an illustration of the reflecting radiation force balance target. The target itself is a Plexiglas rectangle with a small cavity. Glued with a watertight seal to the Plexiglas surface is stainless steel shim stock approximately 13 μm thick. This creates a sealed air cavity. Attached to the backside of the target to counteract partially the buoyancy created by the trapped air pocket are lead weights. Proportion of these weights is such that the target sinks stably.

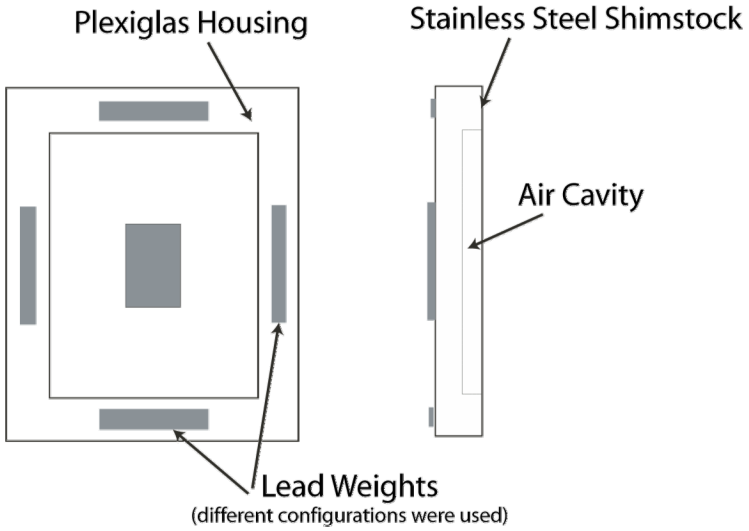

Figure 2-2: Radiation force balance reflecting target

With this construction, the target provides a perfectly reflecting surface because of the impedance mismatch between the trapped air and the water. Targets with various sizes of air cavities have been built for experimentation. These cavities need to be large enough to intercept the acoustic beam fully, even as the target deflects.

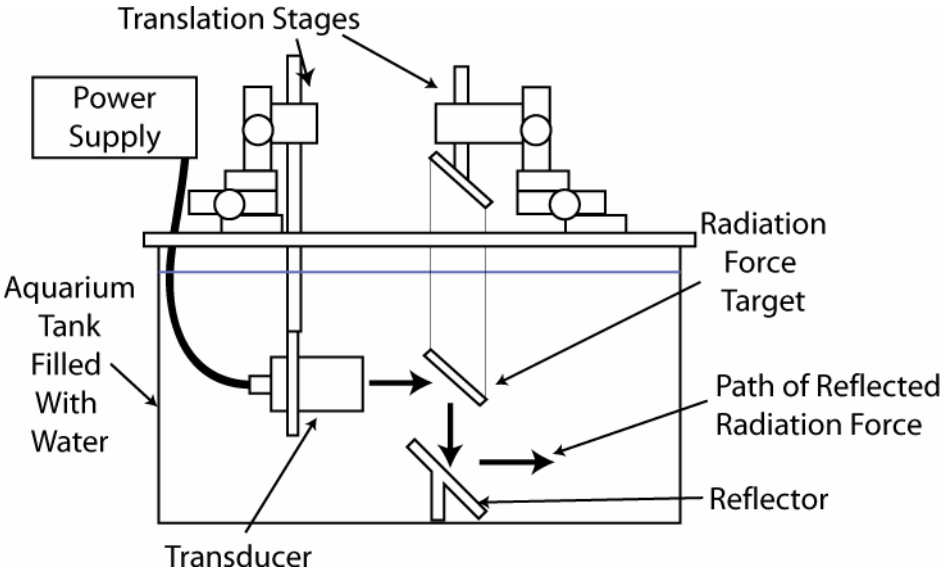

Figure 2-3: Calibration tank setup

The target was suspended to maintain a 45-degree angle in the field of the acoustics (shown in Figure 2-3). This figure shows that as an incident wave encounters the target, it reflects through 90º where a stationary reflector again reflects it into the back of the tank so it will no longer affect the target. The reflector is a hollow Plexiglas box weighed down to counteract the effects of buoyancy.

The typical suspension length of the filament is around 350 mm. Targets of different sizes and weights were used to hold the deflection of the target at less than 20 mm. This allows the target to maintain an approximate 45-degree orientation as it deflects as long as all four of the filaments are taut. Additionally, a small angle approximation can be made that will aid in calculation of radiation force. (See Table 2-1)

Measured Deflection (mm)	*Arc Traveled (mm)*	*Angle Created (°)*	*Small Angle Approximation (°)*
1	1.00000	0.16370	0.16370
2	2.00002	0.32741	0.32740
3	3.00007	0.49112	0.49111
4	4.00017	0.65484	0.65481
5	5.00034	0.81857	0.81851
6	6.00059	0.98231	0.98221
7	7.00093	1.14607	1.14592
8	8.00139	1.30985	1.30962
9	9.00198	1.47364	1.47332
10	10.00272	1.63747	1.63702
11	11.00362	1.80132	1.80072
12	12.00470	1.96520	1.96443
13	13.00598	2.12911	2.12813
14	14.00747	2.29305	2.29183
15	15.00919	2.45704	2.45553
16	16.01115	2.62106	2.61924
17	17.01338	2.78513	2.78294
18	18.01589	2.94924	2.94664
19	19.01869	3.11340	3.11034
20	20.02180	3.27761	3.27404

Table 2-1: Verification that a small angle approximation is appropriate for a hanging length of 350 mm

Targets of different sinking weights were developed. A light target was the most sensitive; however, using such a target with a large radiation force will deflect the target out of the measurement range. If a target is too light, it can also be "pushed" by the radiation force so that the hanging filaments do not remain taut. Conversely, heavy targets will provide little sensitivity for small radiation forces but are needed when larger forces are being investigated. The goal in manufacturing (or deciding on a previously manufactured) target is to get the maximum sensitivity for the tested acoustic field. After choosing a target with the appropriate characteristics, measurement of radiation force could commence.

2.4.3 Deflection measurement

After placing a radiation force target appropriately in an acoustic field, radiation force encounters the target and causes deflection. By measuring the value of this deflection, the magnitude of the force can be determined. The design of these targets allows them to be very sensitive to radiation force, and thus requires a precise method to measure the deflection. To do this, the target is labeled with a small reference dot, and the researcher must define how far the target has displaced by measuring how far the reference dot moves in the x direction upon interaction with the radiation force.

Because the goal of the system is to be as sensitive to radiation force as possible, removal of the operator from all apparatus will help to eliminate disruption with any measurement. A black and white CCD camera with an appropriate zoom lens attachment visualized the target. This lens allowed for focusing, zooming in and out (up to 20x), and adjusting contrast. Before display of the image produced by the camera on a television monitor, the signal was fed through a crosshair generator that placed stationary, locating cross hairs on the presented image. What resulted from this setup was a system that relieved eyestrain and allowed for greater reliability with data readings because of fewer physical interactions by the experimenter with the apparatus that could disturb its accurate placement.

2.4.3.1 Locating the target at the focal distance

To determine the radiation force of a transducer at a given output, the target was located at the focus of the acoustic beam. To do so, a transducer was placed in a testing tank and driven to produce a low level of acoustic field. A Sound Signal at a Point (SSP) was then used to sweep the sound field and locate the focus of the transducer. The position of the tip was located at the crosshairs of the scope. Once completed, careful attention was taken to make sure the camera apparatus was left undisturbed from this location. The SSP was removed from the tank and the target was inserted. The reference dot made during the target's manufacture was then aligned with the cross hairs on the imaging system. Now the target was located at the focal distance of the transducer, however, its center of mass may not coincide with the focal point. The target was moved so that the center of the target was at the focal point of the transducer. To verify placement, a short burst of high-intensity sound was directed towards the target. If the target swung back perfectly, keeping all suspension lengths taut and not rotating, it was determined to be in the center of the pressure field. If any deviation occurred, the focus was not coincident with the center of gravity of the target and some modification in placement must be made. This process was important, as any error in target placement can affect deflection readings.

2.4.3.2 Finding radiation force using the reflecting target

Radiation force will deflect a target. The target is in equilibrium under the action of the radiation force, F_{rad}; the tension in the suspending wires, T_s; and the buoyancy compensated weight of the target, $m_t g$. Summing both the horizontal and vertical directions and recognizing that deflection is a small angle:

$$F_{rad} = \frac{m_t g d}{l + d} \tag{2.9}$$

where d is the target deflection and l is the suspension length. Thus, by knowing the properties of the target (m and l) and by measuring the target deflection, the radiation force can be calculated.

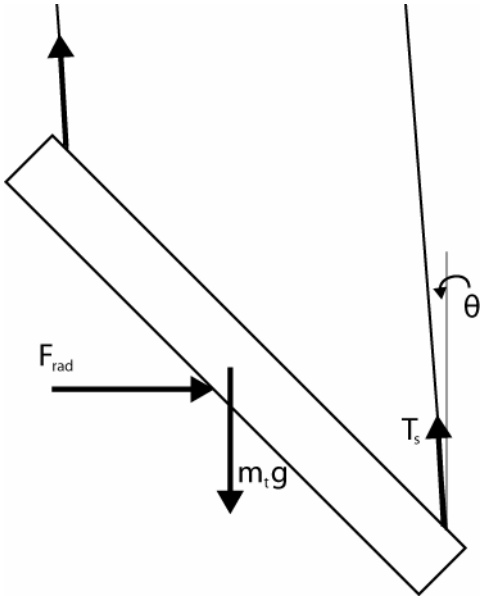

Figure 2-4: Force diagram for reflecting target

Up to this point, this section has touched on radiation force, the apparatus to measure it, and the experimental measurement technique. The next section will build on this study to show the use of radiation force to calibrate an SSP using a reflecting target. The papers of Torr (1984) and Madanshetty and Chandran (2005) are good references for this study. The next section will review the basics of this analysis and follows quite closely the techniques described by Madanshetty and Chandran.

2.4.4 Radiation force calculation to experimentally calibrate SSPs

The radiation force balance technique is an absolute calibration method to measure acoustic power. Section 3.3.3 shows how a properly chosen reflecting target can measure the radiation force of a source acoustic field. This information allows development of a relationship between this force and the acoustic intensity created by the transducer. This relationship will provide a method for absolute calibration of a SSP. This method does not require that the researcher know the calibration constant of either the SSP or the transducer. Only information regarding acoustic radiation force is necessary.

Earlier, equation (2.9) related deflection of a reflecting target to acoustic radiation force. This provides one part of the overall system. Calibration of a SSP requires observation of data that relates deflection to acoustic intensity. In equation (2.4) a relationship was derived for radiation force from an acoustic standpoint. Leighton (1994) provides the equation for acoustic power, $\dot{W}$, as:

$$\dot{W} = I\,A \tag{2.10}$$

Substitution with equation (2.4) shows:

$$\dot{W} = F\,c \tag{2.11}$$

Calculation of the acoustic power output for a given transducer input voltage could be completed by knowing the radiation force (measured by the deflecting target) and the speed of sound in the fluid medium.

Another approach can obtain the acoustic power of a transducer. In this method, an SSP scans the acoustic field at its focal distance to produce a transverse beam profile. (Figure 2-5 shows a typical transverse beam profile.) The properties of the piezoelectric element in the SSP provide that the output of the SSP is directly proportional to the acoustic pressure.

$$p = K_{ssp} V_{ssp} \tag{2.12}$$

The acoustic field is cylindrically symmetric along the central axial direction of the transducer. From the transverse beam profile, the equation for acoustic power is (Chandran, 2000):

$$\dot{W} = (DF)\int_0^R \frac{K_{ssp}^2 \left(V_{ssp}(r)\right)^2}{\rho c}\pi r dr \tag{2.13}$$

where DF is the duty factor of the acoustic wave.

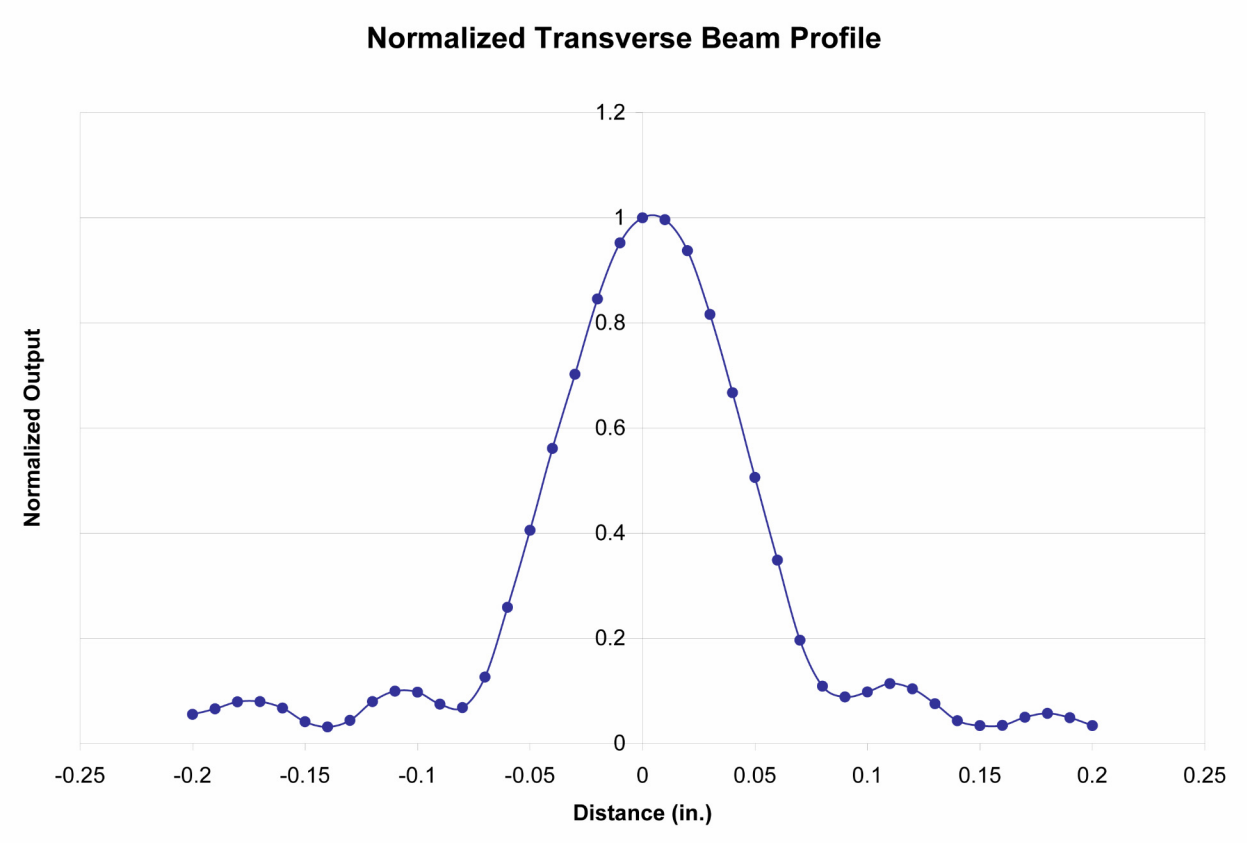

Figure 2-5: A typical transverse beam profile of a transducer

If the transverse beam profile in equation (2.13) is measured at the same driving voltage as the deflection in equation (2.11), then these two measures of acoustic power can be equated. This produces an equation with the only unknown being K_{ssp}, the constant of proportionality between voltage and pressure of the SSP.

2.5 The calibration constant

The previous section shows the absolute calibration method of the SSP using the second order effect of radiation force. This measured calibration constant (K_{ssp}) is unchanging for a specific SSP. Verification of this fact occurs by equating (2.11) and (2.13) at different driving voltages and solving for the unknown K_{ssp}. A calibrated SSP can calibrate a transducer.

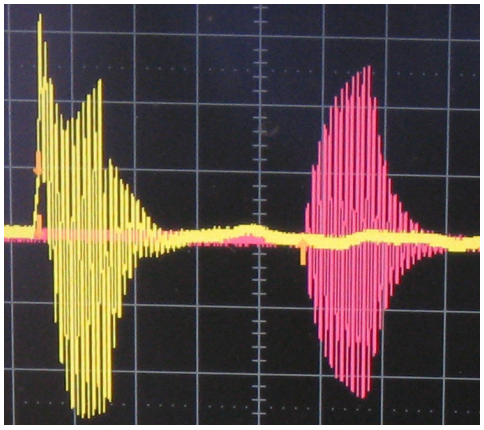

Figure 2-6: The transducer (yellow) and SSP (pink) oscilloscope traces

Figure 2-6 shows the transducer driving voltage and the resulting SSP voltage trace. Measuring this relationship at different driving voltages produces a graph similar to that presented in Figure 2-7. Since the slope of the graph is first order, the calibration value of the transducer (K_{trans}) can be determined. Measurement of this relationship can only occur directly at low values because of cavitation.

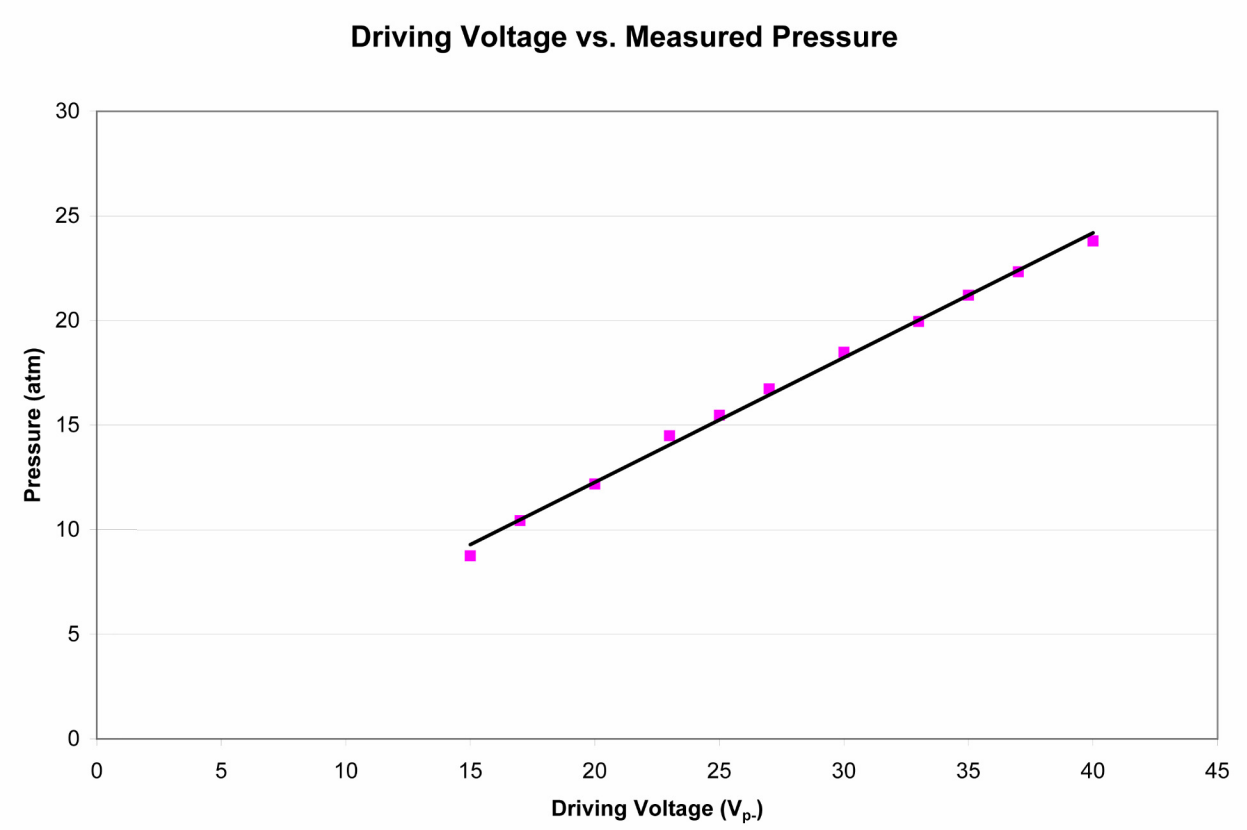

Figure 2-7: SSP measured pressure produced by a transducer at different driving voltages

To show that the SSP measured calibration constant of the transducer is valid above the cavitation threshold, the radiation force target is used. To do so, the deflection of the radiation force target is measured at increasing transducer driving voltages. Because:

$$\text{Radiation Force} \propto \text{Target Deflection} \tag{2.14}$$

and:

$$\text{Radiation Force} \propto \left(\text{Driving Voltage}\right)^2 \tag{2.15}$$

Experimental measurement of data producing a first order graph of target deflection vs. the square of transducer driving voltage, allows the acceptance that the calibration constant of the transducer measured at low intensities is valid above the cavitation threshold.

2.5.1 Acoustic streaming

At high acoustic intensities, the deflection of the radiation force target may not be solely due to radiation force, but the additional second order effect of acoustic streaming. Chapter 3 will provide more insight into the subject, but a brief introduction follows. At high acoustic powers, the fluid around the focus of the transducer can begin to stream. This flow can itself deflect a target along with the radiation force[3]. If subtraction of the deflection caused solely by the streaming flow from the deflection measured by the radiation force target does not occur, an accurate relationship cannot be made.

Streaming measurement requires the manufacture of an appropriate streaming target. Recall that with the radiation force target, a cavity was machined out of Plexiglas and then a thin sheet of stainless steel covered this cavity to produce a reflecting surface. A streaming target only required the creation of a Plexiglas frame. Acoustically transparent Mylar stretched in the center of this frame (much like a window screen stretches over its frame). Therefore, with this target, the acoustic wave encountered only Mylar as it traveled in the fluid. Since Mylar is acoustically transparent, when ultrasound encounters the target radiation force (a purely acoustic phenomenon) will not deflect it. However, Mylar will capture the effect of the streaming flow and the target will deflect. It is important to manufacture the streaming target to be the same size

[3] It is interesting to note that Dvorak quite possibly made the first measurement of acoustic radiation force in 1876. Eckart believed in 1938 that this measurement was not radiation force, but rather streaming (Rooney, 1988).

and weight as the radiation force target to provide comparable experimental data. With such a target measuring pure streaming, subtraction of this streaming only deflection from the total deflection found with the radiation force target will find the true value of radiation induced deflection.

In order to verify that the streaming target is acoustically transparent, a SSP was placed at a specified distance past the focus of the acoustic transducer. The received voltage of the SSP was recorded. The streaming target was then introduced between the SSP and the transducer, and the received voltage of the SSP was recorded again. It was experimentally observed that these values do not differ; thus, all acoustic energy passed through the streaming target.

2.5.2 Experimentally showing K_{trans} applicability

Using an appropriate radiation force target, deflection measurements were made at different transducer driving voltages. Figure 2-8 presents representative results of this study. This relationship shows that the calibration constant (K_{trans}) is valid beyond the low range directly measured.

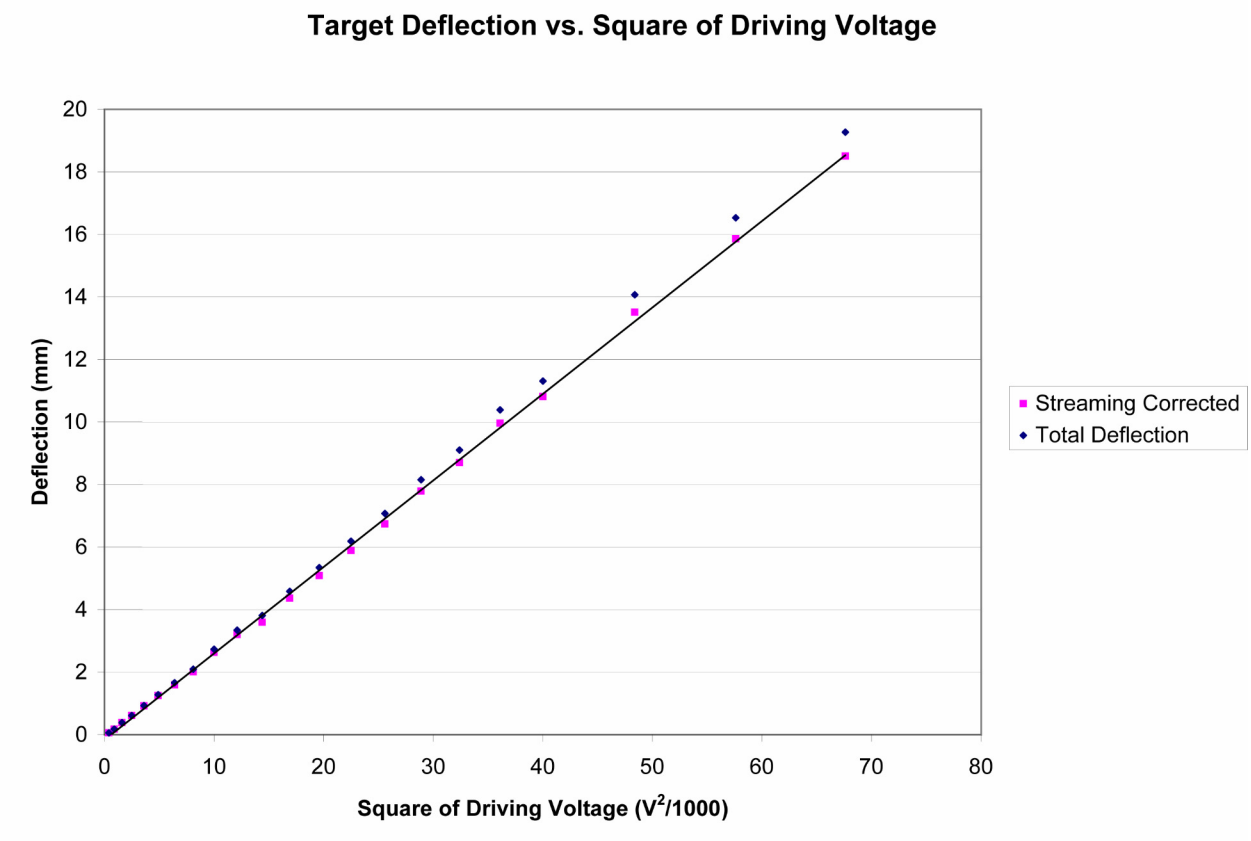

Figure 2-8: Radiation force target deflection vs. square of driving voltage

2.5.3 Cavitation events in radiation force measurement

During the experimental data collection to determine the relationship between driving voltage and deflection, cavitation events interacted with the target. These cavitation events began occurring at a driving voltage of 100 V_{p-}. The photograph in Figure 2-9 shows a typical cavitation trace received by an oscilloscope. Cavitation events continued to occur sporadically as driving voltage increased. At a certain point, cavitation no longer occurred in singular events but rather simultaneously in what will be described as clouds. These events produced an audible noise and could be seen by the naked eye in the water (Figure 1-6). The occurrence of these events caused the radiation force target to have pulses of movement that would disrupt it from its normal steady-state deflection. At a certain point, these cloud-like events occurred closer together, and the target was never steady and could be described as "fluttering." In order to assure that the data being read from the target were correct, data taking was discontinued at a point when cloud events occurred closer than 15 seconds apart. When the events were spaced more closely, the target did not have time to settle to a steady-state value able to be measured. When this rate of cloud cavitation occurred, data taking with either radiation force or streaming targets ceased.

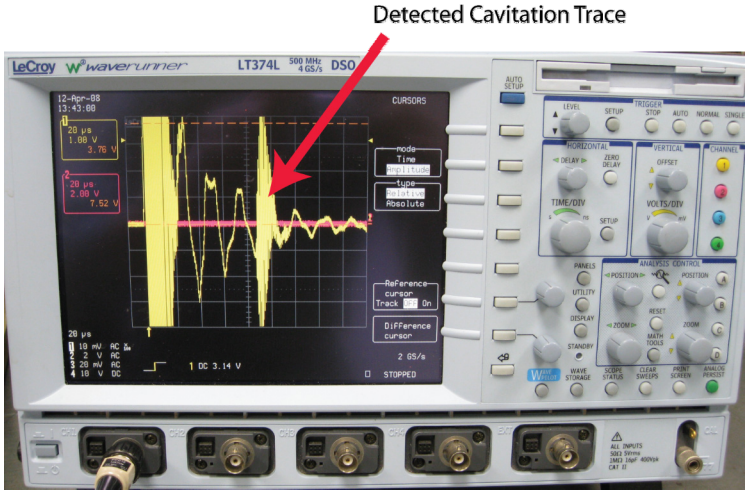

Figure 2-9: Cavitation detected on oscilloscope

2.5.4 Force of a single cavitation event

Because of the influence of cavitation, additional experiments determined if a singular cavitation event added any measurable force to the target to increase its deflection. Using the target in this study (of medium size and 1.8 gm), repeated cavitation events (as visualized on the

oscilloscope) did not add any deflection to the target. To further show that singular cavitation events would not alter the data, a much lighter target[4] was chosen. Using the least count of the traveling microscope (0.01 mm) and making a projection using equation (2.9), the minimum force that could be measured with this light target was 0.24 μN. Using a testing system with these attributes produced no measurable deflection when a cavitation event occurred.

Measurement was attempted under many situations; however, changes in the frequency or intensity of the singular cavitation events resulted in no additional deflection. However, when cloud cavitation occurred there was a change in deflection caused by the burst of those events. Chapter 4 will further investigate this topic to see if information about the energy of a single cavitation event can be estimated.

2.5.5 Lobe-Voltage technique

The radiation force balance method experimentally establishes the calibration of a transducer to be constant over a range of driving voltages. However, in this deflection-based method, the SSP is not used to directly measure the output of the transducer. To provide a direct measurement, a technique called Lobe-Voltage is used. As shown in Figure 2-5, the transverse beam profile of the acoustic beam at the focal distance shows a maximum at the focus and two symmetrical lobes[5] on either side of this focus. A SSP provides an opportunity to measure the acoustic field at a lobe and not be substantially affected by the high intensities (and correspondingly the damaging cavitation) that occur in the focal zone. Therefore, the Lobe-Voltage technique can provide a relationship between measured voltage at a lobe and the intensity at the focus.

Figure 2-10 shows the experimental setup. A fixture that allowed for easy movement and orientation holds a transducer. Once placed in a desired location, the transducer was held stationary and locked in place. The SSP was located opposite of the transducer and held in an appropriate fixture attached to a three-axis translation stage. This allowed proper placement of

[4] 0.8 gm – the lightest buoyancy corrected target that could be made to still accurately measure force.

[5] The lobe described is an area outside of the focus that has a measured local maximum.

the SSP in the focus of the transducer. It was important that the SSP be oriented perpendicular to the transducer's face and its traverse follows a parallel path to that face.

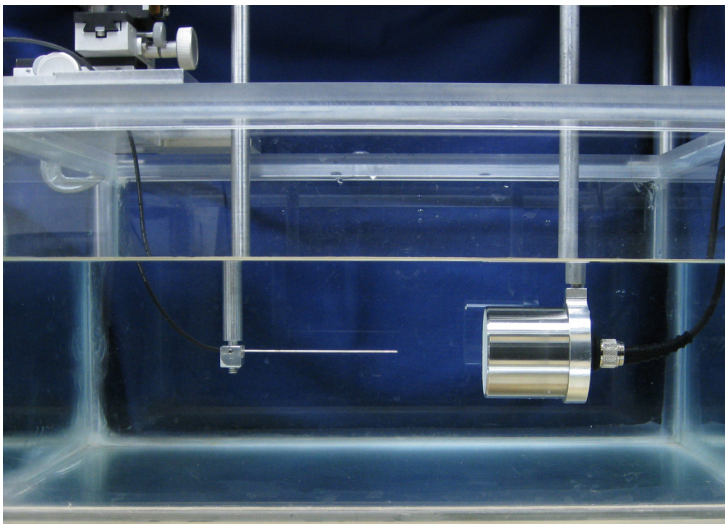

Figure 2-10: Using an SSP to measure transducer output

Using a calibrated SSP, readings were taken of the transducer at three points: the focus, the first lobe, and the second lobe. The test was completed with a previously calibrated transducer, so it was known what driving voltage to the transducer should produce cavitation at the tip of the SSP. When collecting data, it was found that when the SSP was placed at the first lobe of the transducer, the SSP was substantially affected (the voltage received fluctuated) by cavitation created at the focus after focal intensities reached 1200 W/cm^2. At this point data taking discontinued. Similarly, data collection at the second lobe stopped at an intensity of 2750 W/cm^2 due to fluctuation of the voltage received.

Figure 2-11 shows that the relationship between focal intensity and the square of the voltage measured at the lobes is linear. This relationship allows creation of an appropriate sensitivity factor (K_{lobe}) to calculate the value of the intensity at the focus by directly measuring voltage output of the lobe.

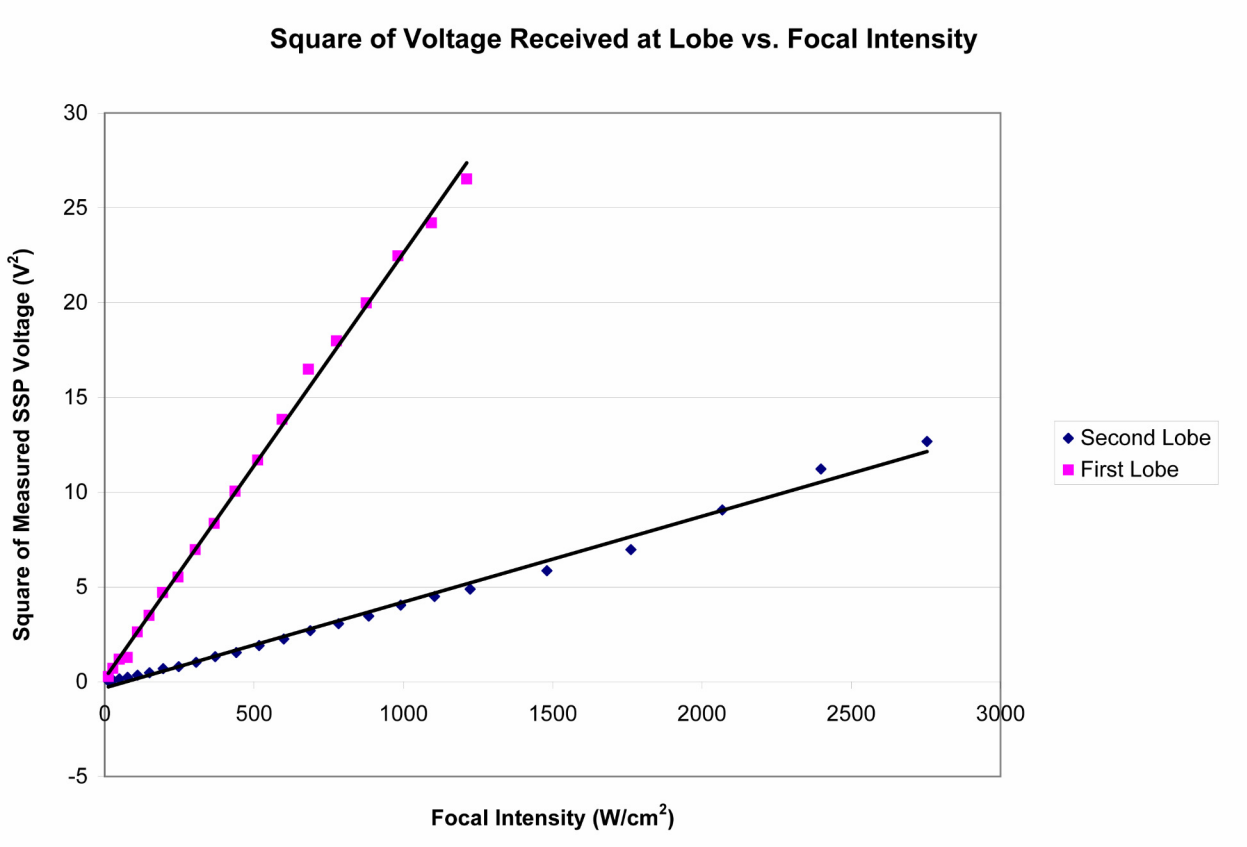

Figure 2-11: The square of lobe pressure measured by an SSP vs. focal intensity

2.6 Summary

Many experiments with high-intensity, focused ultrasound produce cavitation events. The production of cavitation makes a direct measurement of pressure using reference hydrophones because it can damage these sensitive devices. Resolving this problem required the design and in-lab manufacture of a needle hydrophone called a Sound Signal at a Point (SSP). Calibration of the SSP occurred through a standard method of radiation force balance. This SSP provided the same quality as, but is less expensive than, commercial reference hydrophones and provides researchers with more freedom in experimentation.

A SSP can calibrate a transducer. This calibration must be completed at low values of intensity due to cavitation. It was experimentally observed, using the technique of radiation force balance, the applicability of the transducer's calibration constant up to a point where cloud cavitation disrupts the experimental apparatus. This applicability was also confirmed using the direct measure of the Lobe-Voltage Technique.

Chapter 3 - Acoustic Streaming

As shown in Chapter 2, the second order effect of radiation force is a subtle effect of a high intensity sound field. The measurement of radiation force is a delicate operation. When properly created, high intensity acoustics can create the related second order effect of acoustic streaming. This streaming will affect a radiation force target. Acoustic streaming is the process of time independent flow in a fluid medium. Like cavitation, acoustic streaming is a process that a researcher in acoustics must consider especially in those instances mentioned earlier in the radiation force balance. This chapter will provide an experimental look at streaming in the context of high frequency, focused, pulsed, high-intensity acoustic fields.

3.1 The study of acoustic streaming

Researchers present different arguments as to when the study of acoustic streaming began. Nyborg (1965) states that Faraday first observed what is now called acoustic streaming in 1831 when looking at air currents that rose at points of maximum vibration amplitude of plates. Some authors point to Rayleigh (1884) when he looked at the problem of a standing wave between parallel walls. Starritt (1990) states the first recording of acoustic streaming was in 1926 by Meisner when he reported that fluid appeared to be sucked into a sound beam at a vibrating quartz crystal and set into motion in the direction of the wave propagation. Fortunately, what matters is not the initial observation but the body of work completed to understand more fully the phenomenon.

The study of acoustic streaming involves many situations, some involving the interaction of sound fields with boundaries, and others concerning the propagation of a sound wave in a large space. Application of acoustic streaming varies from research into the removal of particles loosely attached to surfaces, to the biological effects produced with medical ultrasound. Because streaming is a bulk movement of fluid, it can be used as a stirring agent that can aid many applications, specifically those that deal with increase of reaction rates. In addition, streaming has been shown to enhance heat transfer (Nyborg, 1965).

Zarembo (1971) classified acoustic streaming into three types, depending on the scale of the fluid motion:

1) Eckart type – Streaming generated in a non-uniform, free sound field, whose scale is much larger than the acoustic wavelength.
2) Rayleigh type – vortex-like streaming generated outside the boundary layer in a standing wave field, whose scale is comparable to the wavelength.
3) Schlinhting type – vortex motion generated in a viscous boundary layer on the surface of an object placed in a sound field, whose scale is much smaller than the wavelength.

In this dissertation, Eckart type streaming is studied.

Some authors confuse the term acoustic streaming and use it to describe two separate phenomena. Clear distinction should be made between these definitions. First, the use of the words "acoustic streaming" will refer to the bulk fluid movement that results from the presence of a sound wave in a fluid medium. "Acoustic microstreaming" will be used to describe small scale streaming that occurs because of the collapse of cavitation bubbles (Starritt, Duck, & Humphrey, 1989).

3.1.1 Historical review

Since the initial discovery of streaming, no matter the precise date, the study has been far-reaching. In many older texts the phrase "Quartz (or Ultrasonic) Wind" is used to describe the phenomenon of acoustic streaming, because it was originally seen to occur with quartz oscillators. The notion that quartz is the only material that creates this event is incorrect; any high-intensity sound source will generate streaming.

The first theoretical analysis of streaming was produced by Eckart (1948). He showed that the transfer of momentum from a wave to a fluid because of viscous loss generated acoustic streaming. Markham (1952) built upon this theory and replaced Eckart's equation of state with a more general one that took acoustic relaxation effects into account. Using this new equation, Medwin (1954) concluded that it was not simply viscous loss that was proportional to streaming, but additionally attenuation of the sound beam. In their article "On the forces producing the ultrasonic wind," Fox and Herzfeld (1950) argued that all absorption mechanisms for sound waves must lead to streaming and used this to introduce the fact that radiation force was the cause of the streaming or "wind" effect. Using these studies as a background, Piercy and Lamb (1954) developed a theory in which time independent gradients of radiation pressure in the

direction of propagation acted as the driving force for the streaming flow. Tjøtta (1959) showed that by using a method of approximations, an analysis of streaming using Eckart's method of viscous loss can be shown to be the same as that found using a radiation pressure analysis.

3.1.2 Modern research interests

Modern work in acoustic streaming has been in the studies of medicine and biology. The advent of newer commercial systems that use ultrasound at higher intensities has necessitated more research on sound's thermal and mechanical effects. The American Institute of Ultrasound in Medicine (AIUM) has approved an Output Display Standard that requires all ultrasonic systems to have real time display of both "thermal index" and "mechanical index" (AIUM/NEMA, 1992). Since acoustic streaming may occur in the focal length of an acoustic beam, fixed cells may experience shear viscous forces due to nearby streaming fluid flow (urine, amniotic fluid, blood, etc). The possible biological effects must be investigated (Wu & Du, 1993).

3.2 Models for acoustic streaming

Acoustic streaming is the flow resulting from a radiation pressure gradient being set up in a fluid medium. Creation of this pressure gradient occurs by absorption in the attenuating medium that is the fluid. Energy can be lost in an attenuating medium through a few mechanisms. As the waveform travels through the fluid, it encounters viscous forces that oppose its motion. The heat created as the mechanical energy works to overcome this viscosity is a form of energy loss. In a heterogeneous medium, acoustic scattering can also lead to energy loss. Whatever the cause, the momentum that is absorbed from the acoustic wave can lead to streaming flow.

A number of authors have looked at the theoretical problem of predicting streaming flow. These theoretical derivations of streaming equations assume a homogeneous, isotropic fluid in which the pressure, density, and velocity at a point are given instantaneously. Much attention has been paid to creating a model for continuous plane wave acoustic streaming under bounded conditions. Many of these models can be quite complex and involve second-order terms. Using the Navier-Stokes equations and the equation of continuity, a series of approximations obtain a streaming equation. The literature from the researchers mentioned in the last section shows that each researcher has created a slightly different equation to theoretically define streaming. The

differences stem from the origin of the force causing the stream, the geometry of the acoustic source, the boundary conditions, and the nonlinearity associated with the ultrasound propagation. In most cases, streaming velocity relates to acoustic intensity, the radius of the acoustic beam, viscosity, and the absorption of the fluid. Many have geometrical factors resulting from the different boundary conditions used in the solutions.

3.2.1 Models for plane wave acoustic streaming

A considerable amount of literature illustrates the main ideas for the classical analysis of acoustic streaming. These analyses mainly concentrate on plane continuous waves or waves in tubes. In summary of these views, two commonly referred to in the literature will be presented. Eckart (1948) is probably considered the building block of all of these studies, as his paper provided the earliest theoretical analysis. He concluded that streaming was produced because of the transfer of momentum from the waveform to the fluid. This theory was extended, most notably by Nyborg (1965), to state that streaming was caused both by the loss of acoustic momentum and by attenuation of the sound beam. Nyborg's analysis is the one most generally referred to by researchers in the field. In all derivations the assumption is made that the acoustic wavelength is small when compared to the beam width; the effects of diffraction can therefore be neglected.

3.2.2 Eckart's solution for streaming flow

Eckart derived a streaming equation for a non-divergent sound beam in a cylindrical tube of sufficient length for end effects to be neglected. This analysis provided:

$$v = \frac{\alpha I}{\mu c} r_1^2 M \qquad \textbf{(3.1)}$$

where v is the velocity, α the absorption coefficient, r_1 the radius of the tube, and M a geometric factor related to the radius of the tube and the sound beam. Eckart obtained an order of magnitude estimate of streaming velocity by setting M = 1 (Starritt, 1990).

3.2.3 Nyborg solution for streaming flow

The analysis of Nyborg (1965) is possibly the most referenced in the study of acoustic streaming. He bases his analysis on the non-linear wave equation and the Navier-Stokes

hydrodynamic equation. He states that the maximum streaming velocity, *v,* in a situation where the attenuation coefficient was much less than one is shown by:

$$v = \frac{(k \cdot r)^2 c \cdot b^*}{4}\left(\frac{U}{c}\right)^2 \tag{3.2}$$

where *k* is the wave number, *r* is the radius of the sound beam, and *U* is the velocity of the wave given by:

$$U = \frac{p}{\rho c} \tag{3.3}$$

and

$$b^* = \frac{1}{\mu}\left(\mu' + \frac{4}{3}\mu + \rho R\right) \tag{3.4}$$

where R described the relaxation effects of the sound beam (Starritt, 1990).

Nyborg also presented an equation to describe the radiation pressure gradient, ∇P. Here the absorption coefficient factor is represented by α. The radiation pressure gradient on the particle will be (Nyborg, 1965)

$$\nabla P = \frac{I\alpha}{c} \tag{3.5}$$

Equation (3.5) makes it clear that intensity and attenuation of the fluid can greatly affect radiation pressure gradient. An increase in either of the parameters therefore increases streaming.

3.2.4 Streaming flow in focused beams

It is important to note that the high frequency, high-intensity ultrasound studied in this dissertation differs from those in the classical models because the fields in this research are pulsed, focused, and not a continuous plane wave. Some authors (Wu and Du (1993), Kamakura, et.al (1995), and Nowicki, et. al. (1997)) have attempted to develop theoretical expressions for streaming in focused beams which can be used to predict streaming in water. These expressions tend to be complex but when applied appropriately are said to "adequately" predict "some" experimental measurements (Duck, 1998). Duck also states, "Full theoretical descriptions of such (focused) flows have not been fully established." Kamakura (1995) mentions that "relatively few studies of acoustic streaming induced in focused beams" have been studied.

Additionally the focused models will not apply to this research since they were developed for a focused geometry applied in a continuous wave condition and not one pulsed at low duty factors. Starritt (1989) notes that even though many models have been created, an all-encompassing model that will specifically analyze the conditions of focused, pulsed fields has not been developed.

3.3 Methods of experimentally measuring flow velocities

Research into the magnitude of the streaming velocity for pulsed fields has used a variety of flow velocity measurement methods including but not limited to Hot Wire Anemometry, Doppler Shift, Laser Doppler Velocimetry (LDV), Particle Imaging Velocimetry (PIV), and contrast dye measurement. Each of these techniques has its advantages and drawbacks. Two of the previously mentioned techniques, PIV and contrast dye, will be described and explored along with a method using a streaming target in the experimental section of this chapter. This section gives a description of other available techniques of note.

3.3.1 Hot-Wire anemometry

Hot-wire anemometry bases itself on the principle of measuring heat loss from an electrically heated probe caused by the flow of the fluid around it. These probes must be held at a constant temperature; otherwise, the fluctuations caused by streaming will not be accurately measured. These probes are usually made of platinum or tungsten wire deposited on a quartz substrate and electrically insulated for use in water by a quartz coating. Care is taken to avoid bubbles forming on the probe and causing erroneous readings. These probes are calibrated by connecting them to a computer-controlled translation stage and dragging them through the water at a range of velocities and noting the voltage output (Starritt et al., 1989). The hot-wire anemometer, while very delicate, can provide an extremely high-frequency response and is often used to help measure highly fluctuating flows.

3.3.2 Doppler shift

The velocity of a fluid flow can be measured using an acoustic Doppler technique. This technique measures the change in frequency of sound reflected by a moving object. This change in frequency is called the Doppler shift and its magnitude, Δf is given by:

$$\Delta f = \frac{kvf}{c} \tag{3.6}$$

where k is a measurement specific constant (depending on the setup used), v the velocity of the reflecting object, f the frequency of the transmitted sound (Dymling, Persson, Hertz, & Lindstrom, 1991). This Doppler shift technique has been used as a non-contact way to measure fluid properties. An interesting application of this method of acoustic Doppler shift was used by Dymling, et al. when they created streaming in milk and were able to determine when it soured by determining the change in viscosity due to differences in acoustic streaming.

3.3.3 Laser Doppler velocimetry

Laser Doppler Velocimetry (LDV) has two models of application. In the fringe model, two optically coherent, thin laser beams are crossed in particle-seeded flow under investigation. The overlapping regime of the crossed beam is the test volume. Because of optical interference between the two coherent light beams, a set of straight interference fringes is set up in the test volume. These fringes are set up to be perpendicular to the flow. As particles pass through the fringes, they scatter light (only from the regions of constructive interference) into a photodetector. The frequency of the scattered light is Doppler shifted and referred to as the Doppler frequency of the flow. This Doppler frequency is proportional to a component of the particles velocity, which is perpendicular to the planar fringe pattern produced by the beam crossing. In order to obtain three components of velocity, three sets of fringe patterns need to be produced at the same region in space. (Merzkirch, 1987) In the Doppler frequency shift, interpretation of LDV the scattered light is regarded as coming from two beams. Optical heterodyning of the scattered light results in a different frequency, which is proportional to the particle velocity. (Drain, 1980) Under appropriate conditions, the governing equation, which can be derived from either interpretation, reduces to:

$$f = \frac{2u \sin\theta}{\lambda} \tag{3.7}$$

where λ is the laser wavelength, u the particle velocity, and f the signal frequency. By measuring this frequency the flow velocity can be determined.

3.3.4 Schlieren methods

Schlieren flow visualization bases itself on the deflection of light by a refractive index gradient. The index gradient directly relates to flow density gradient. Using a set of finely ground spherical mirrors, light from a point source passes through the area of flow and on to a viewing screen. A knife-edge partially blocks the light. The light that is deflected toward or away from the knife-edge produces a shadow pattern depending upon whether it was previously blocked or unblocked. This shadow pattern is a light-intensity representation of the expansions (low density regions) and compressions (high density regions) which characterize flow (Merzkirch, 1987). The main use of flow visualization is in situations with thermodynamic flows. Because this system requires proper illumination, it must be completed in a dark environment and thus causes some problems with setting up a proper experiment due to limited visibility.

3.4 Experimental study of streaming flow

As discussed previously, there are many methods to measure acoustic streaming. This section provides the results of the experimental testing of three methods: Particle Imaging Velocimetry (PIV), contrast dye velocity measurement, and a method using a streaming target. The first two techniques are flow visualization techniques using direct measurements of streaming, while the third relies on deflection analysis to calculate the velocity from a technique similar to the radiation force measurement discussed in Chapter 2.

In this study, investigated was the effect of the pulse width. Even though specific duty factors are used, there is not one specific way to create a particular duty factor. By varying the number of cycles in a pulse, the pulse repetition frequency (or pulse rate) of a desired duty factor can be created in a plethora of ways. The following table shows the parameters for duty factor creation. Explored were duty factors from 1% to 5% because lower duty factors did not produce streaming until very high intensities were applied. In Table 3-1, the left hand vertical column gives the duty factor. The top two rows provide information on the pulse repetition frequency (PRF) and burst period. The body of the table provides the number of acoustic cycles needed to produce a duty cycle with the desired PRF.

	PRF (Hz)	1000	500	333	250	200	100	50	25	10
	Pulse Period (ms)	0.001	0.002	0.003	0.004	0.005	0.01	0.02	0.04	0.1
Duty Factor	1%	12	23	35	46	57	115	230	462	1150
	2%	23	46	69	92	115	230	460	924	2300
	3%	35	69	104	138	173	345	690	1382	3450
	4%	46	92	138	184	230	460	920	1842	4600
	5%	58	115	173	230	288	575	1150	2302	5750

Table 3-1: Function generator settings in order to provide select duty factors created multiple ways for 1.15 MHz acoustics

3.4.1 Dye velocity measurement

Velocity measurement using dye requires the injection of a contrast agent into a fluid. The movement of that dye over a set time is directly measured. A problem with dye tests is that the container in which the experiments are conducted must be flushed on a regular basis. If this is not completed, the contrast between the flow and the background water can become less intense and harder to measure. This problem is only an annoyance, but can cause frustration when taking significant amounts of data.

A variation in dye measurement uses thymol blue indicator to measure flow. The advantage of using this indicator is that the release of color is controllable and reversible (Merzkirch, 1987). The range of color change for thymol blue is between yellow at a pH of 8.0 and blue at a pH of 9.6. Electrolysis controls the pH of water, making this neutral solution become acid near the anode and alkaline near the cathode. To demonstrate streaming, the cathode is positioned across the axis of the acoustic beam at the desired location to visualize streaming while the anode should be placed at the opposite end of the fluid tank. Starritt (1990) used this technique to visualize flows and noted that "because the blue dye consisted of thymol blue ions in solution, the flow was convincingly shown to be the fluid flow rather than particle movement within the fluid." This technique allowed for long testing trials since the thymol blue faded to a yellow color as it traveled from the cathode. Unlike a regular dye, the solution did not have to be replaced to facilitate better contrast.

The study presented in this dissertation used a dye contrast agent created by a potassium permanganate solution. Besides being the author's favorite color of deep purple, the potassium permanganate provided easy visualization of the flow. As noted previously, over time this deep purple color produced a lavender background in the water and required replacement of the water at regular intervals.

A testing column made of a transparent acrylic material and was approximately 8 inches long held approximately 350 ml of water. This column had a small volume of water that was easy to refresh and could provide a more quiescent water sample than a bigger tank might allow. Additionally, the relatively small volume allows the researcher to easily locate the focal distance (where streaming is a maximum) of the transducer.

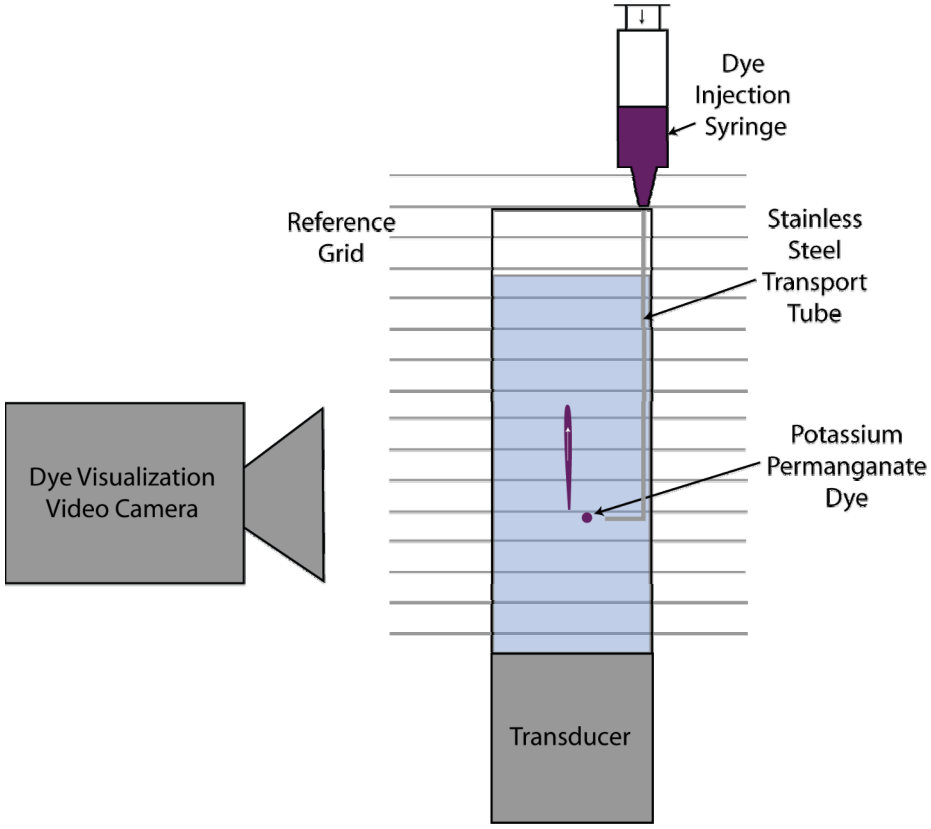

Figure 3-1: Illustration of the dye visualization system

To inject the dye into the focus an effective device was made and repeatable procedure followed. For dye injection, the nozzle of a 10 cc plastic syringe was retrofitted to accommodate a piece of 0.073 inch diameter stainless steel hypodermic tubing. This rigid tubing was then bent at a 90 degree angle to produce a three quarter of an inch bend extension. The length of this bend was such that it would not be responsible for any bend-generated secondary flows. What this effectively created was a syringe with a very long nozzle (approximately seven inches) for injecting dye into the focal zone of the ultrasound.

This syringe was a removable part of the system to allow for easy replacement of the dye. A rigid setup was explored, but it was found that a condition allowing the removal of the syringe was much more effective than one rigidly placed. This produced problems on how to repeatedly

locate the syringe so that it would inject dye into a consistent area, namely the focus of the acoustics. To solve this problem, a reference indexer was secured above the column that allowed for temporary, accurate placement of the syringe assembly. To initially locate the distance to which this reference should be positioned, an oscilloscope was used to find the location of the focus (by finding time delay of a reflected signal from the hypodermic tubing).

After the initial locating of the focus, it was important that the tip of the hypodermic tubing did not get into the focus of the acoustics, as this would produce cavitation. Cavitation could produce turbulence that would negatively affect the measurement. Because of this, the syringe extension bend was *at least* three focal diameters away from the focus. The researcher could then manipulate the syringe to create a dye flow that injected directly into the focus. At some points this flow was a continuous stream of dye, but it was found most useful to produce a small burst (this also could be described as a glob or bubble) of dye. When the streaming flow hit this burst, it would completely stream the dye and provide results to read and measure.

Data of streaming velocity using dye could occur two ways: by timing the flow over a set distance using a stopwatch or by videoing the flow over a reference grid and then analyzing the video frame by frame. Because the stopwatch method provided large errors at high velocities, the video camera was the method used. A set of lines, spaced at intervals of one centimeter, were placed directly behind the transparent column. The video camera was oriented in front of the column and centered so that it captured the area around the focus of the transducer where maximum streaming occurred. When testing commenced, video was recorded while the experimenter injected bursts of dye into the focal zone. Dye bursts hitting the focal zone created a dye trace. This procedure was continued for a round of tests or until it was felt the background water did not provide enough contrast and needed replacement.

The recorded data was analyzed by using Adobe Premiere video editing software. In this software, a template overlay was created that allowed for precise measurement of the flow velocity. This overlay was based upon the one-centimeter reference measurements provided during the experiment and was made so that it gave finer gradations in quarters of centimeters. Because it was known from reading multiple references (Starrett, Duck, etc.) that the streaming velocity would decrease as the distance from the focal zone increased, the measurement readings were only taken from the focus to a distance of two centimeters. Even at this short distance, some decrease in streaming velocity may occur. The video editing software could advance the

video frame by frame and still accurately determine the time of flow because of the video time code. This method of data analysis provided more accurate results than simple eye and stopwatch methods.

3.4.1.1 Dye test experimental results

The dye measurement technique was not sensitive to streaming flows in the mm/s range. Low velocity streaming was seen but could not be accurately measured using the frame-by-frame analysis. The minimum velocity available to be measured set the minimum intensity to be tested. If the intensity applied to the water medium was too high, cloud cavitation would form causing vortex-like patterns and immeasurable streaming values. Between these two values (low – where the streaming was first visualized. and high – where cloud cavitation formed) large intervals had to be used between the intensities investigated in order to distinguish between velocities. For example, with a 1% duty factor, velocities at 1677 W/cm^2 and 1925 W/cm^2 could not be distinguished confidently; however, those between 1677 W/cm^2 and 2190 W/cm^2 could be distinguished.

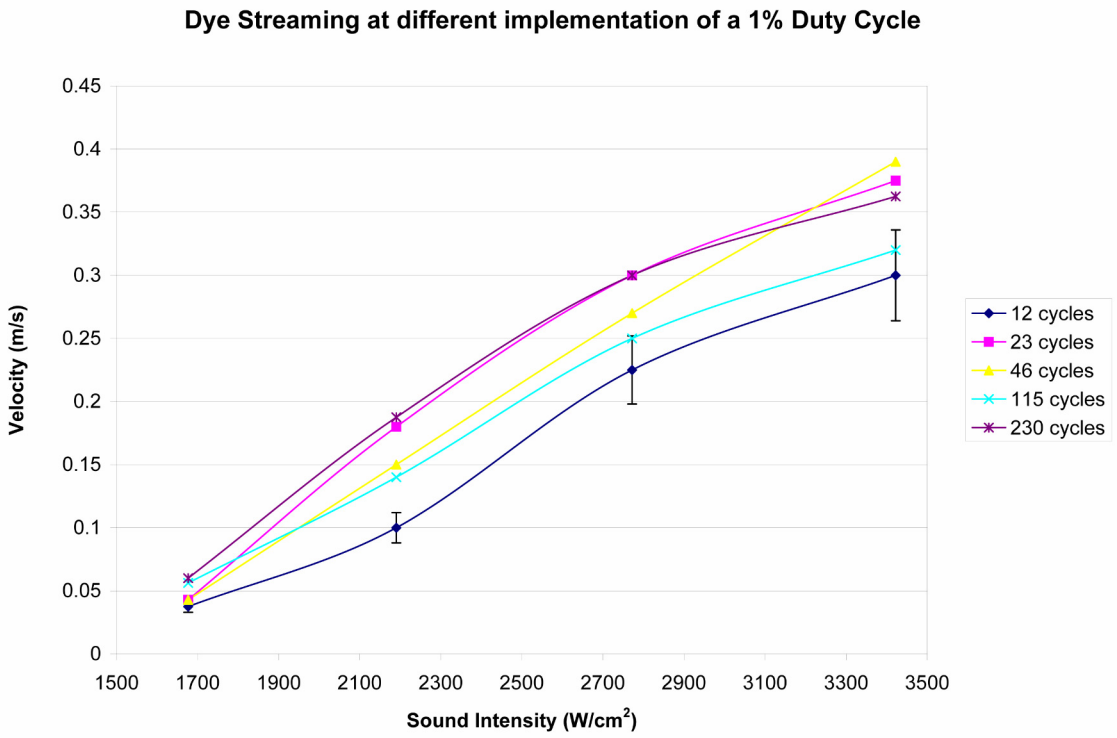

Figure 3-2: Dye measured streaming velocity profiles at a 1% duty factor implemented different ways

Figure 3-2 shows the data found from streaming at a 1% duty factor. Each line represents the duty factor created with a different number of cycles. Representative error bars are shown for the 12-cycle case. The duty factor was created using the values given in Table 3-1 using five specific pulse widths. The graph shows that as intensity increases, the streaming flow does as well. The effect of pulse width did not present itself in this study. Using other measurement techniques, the effect of pulse width will be monitored.

3.4.1.2 The effect of cavitation

At low acoustic intensities (lower than 1600 W/cm^2) limited dye movement was observed. As mentioned, reliable measurement of this movement by the video system was difficult. However, at these intensities, when placing the tip of the syringe at the focus, cavitation would occur at the tip and carry the dye away with a significant velocity. The streaming produced was difficult to measure because it moved from the tip in a turbulent pattern. This was the same effect that was noted when the intensity rose to a high level. Here, cavitation events became more and more frequent until they became sustained and cloud-like. The visualization of cavitation-induced streaming at low intensities shows creation of that significant — although immeasurable — flows.

3.4.1.3 Dye streaming summary

The use of dye in a streaming flow was informative and gave general trend data, but due to the difficulties in accurately measuring the flow, it is not the optimal technique to measure acoustic streaming. This basis led to the investigation of other techniques to visualize streaming. In particular, the Particle Image Velocimetry (PIV) method was of interest because it should be able to measure low velocities that the dye method cannot.

3.4.2 The PIV system

Particle Image Velocimetry (PIV) is a widely used technique to find the velocity of flows. This optical, non-intrusive method of observing flows has been used for decades. PIV is a system of particle seeding, illuminating, and image capturing. This system is more complex than a basic dye system and requires some level of training to understand the operation and procedures required to take good data. Even a well-trained technician can find that capturing streaming flows can be tedious and susceptible to similar microstreaming events such as the dye

tests. The PIV system used in this study is located in the Center for Complex Flows at Kansas State University. At the time of testing, Dr. Steven O'Halloran was the main operator of the equipment and provided training, guidance, and his expertise in setting up the experiments.

3.4.2.1 Dye vs. PIV

Observations in the dye test helped to conclude that there was only measurable movement of streaming flow in water at high intensities or at low intensities due to syringe tip placement in the focus causing cavitation. Repeated tests allowed observation of some slight movement at lower intensities, but below the threshold the apparatus in the dye test could measure. Measurement of these velocities should occur due to the finer resolution of PIV.

PIV measurement of acoustic streaming offers advantages over the dye based method. PIV uses a "cleaner" setup. There was no need to inject or disturb the fluid medium during the test other than filling the host liquid with hollow glass sphere tracer particles of a set diameter. The use of such particles introduced uncertainty as to whether they would affect the acoustics and introduce measurement-changing cloud cavitation.

To determine if the tracer particles would cause experimental problems first, a cleaned column (like that used in the dye tests) was filled with water and the background water cavitation threshold of the water determined. This step showed that the system before the introduction of the tracer particles produced valid results consistent with those previously collected in other research (Wanklyn, 2006). Next, a small amount of tracer particles (TSI brand 10-micron glass filled beads) was introduced into the column. In a PIV test, the amount of tracer particles are not measured but rather optically verified to be of the approximate number density using a high power green laser sheet to illuminate the test cell. Because of this, a similar measure of the amount of tracer particles introduced in the cavitation threshold test setup occurred and verified to be approximately the same amount used in PIV testing. To help in optical verification a laser light sheet created by a modified green laser pointer as shown in Figure 3-3 was used. Once the distribution of particles was sufficient, the test commenced.

The acoustic threshold testing showed that the cavitation threshold of the water filled with tracer particles was lower than that of the background water (cavitation occurred at a peak negative pressure closer to zero). Single cavitation events continued to an intensity where these events crossed a threshold and became sustained and cloud-like. From the dye tests, this caused turbulent flow, so intensities above this value were avoided in the PIV study to get proper results.

As previously mentioned, accompanying these cloud-like events was a recognizable sound. Therefore, even though the PIV experiments would be ran below the cloud cavitation threshold, if cavitation noise was heard, the trial could be stopped so that faulty data would be avoided.

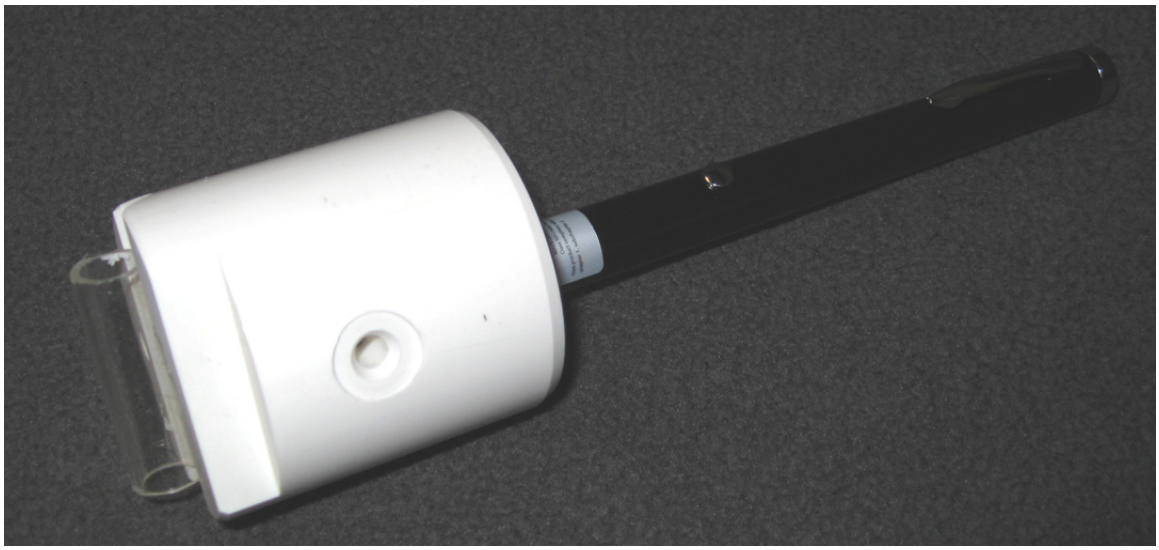

Figure 3-3: Modified green laser pointer to create a light sheet

To further understand the effect of tracer particles in the system, dye tests were attempted with the inclusion of tracer particles to determine if their addition would provide any modification to the flow characteristics as measured by the dye. These trials were ran identically as they were for dye alone. These experiments verified that at low intensities the same noticeable but immeasurable flow did not occur, just as in the tracer particle free case. The only change that the addition of particles created was a lowering of the cloud cavitation threshold (as previously mentioned).

3.4.2.2 Laser and camera alignment

This section will describe the setup of the PIV system in order to take acoustic streaming velocity data. The initial expectation was that streaming could be measured in a column like that used for the dye testing; however, the column produced optical distortion that did not allow this possibility. Thus, the data was taken in a 15-gallon test tank. A transducer mounted to a translation stage was introduced into the left hand side of the tank. The illuminating class IV Nd:YAG (neodymium-doped yttrium aluminum garnet) laser with a 532 nm wavelength from the PIV system was located to the right of the tank and was pointed in the general direction of the transducer. A cylindrical lens provided proper laser beam divergence for the setup. This

resulted in a laser sheet that filled the cross section of the aquarium tank. The thickness of this laser sheet was approximately 1 mm.

Alignment of the laser to the focal zone of the transducer was of utmost importance because the maximum flow velocity occurred at the focal distance of the transducer. Through calibration, the transducer used was known to have a focus approximately 2.5 inches from the transducer surface. Although the focal spot ideally would be geometrically centered with the transducer, this is not always the case. This means that optical laser alignment with the transducer geometry alone will not guarantee that the illuminated cross section will include the focus. To resolve this problem, a SSP was inserted into the acoustic field to probe for the maximum acoustic intensity (focus) as in Figure 2-10.

The dual Nd:YAG laser consists of two separate lasers that produce two laser pulses separated by a small time delay. The maximum power of the laser per pulse is 150 mJ. This class IV laser can cause serious eye damage if not following proper safety procedures. This was especially important with the experiment in question. When aligning the laser to the SSP, the laser must be viewed through laser safety lenses. Laser safety lenses are rated by optical density (OD), which is a measure of how much light of a certain wavelength can be transmitted:

$$OD = \log_{10}\left(\frac{1}{T}\right) \tag{3.8}$$

where *OD* is optical density and T is the transmittance (O'Halloran, 2002). It is recommended when using this specific laser that the lenses used have an OD of 7. These lenses transmit only 0.00001% of laser light. This, however, does not make them useful when trying to align the laser, as these glasses transmit virtually no laser light. Special alignment glasses are then used. These glasses have an OD of 2 (having a transmittance of 1%) allowing the user to see a faint trace of the laser and help in alignment. In no situation should the wearer of these lenses look directly into the laser; alignment should be completed by looking indirectly at the laser set at as low a power as necessary to get a faint trace.

Once the laser was oriented so that the light sheet coincided with the centerline of the SSP located at the focus, the visualization system could be calibrated. For the two-dimensional case studied, this was completed with one CCD camera. The camera had a resolution of approximately one mega pixel (1000 (H) x 1016 (W)). It was mounted on a three-axis traverse that allowed for focusing and alignment.

First, the camera was moved until the SSP was in the field of view and focused. The location of the SSP tip (acoustic field focus) needed to be in the vertical center of the image; by moving the traverse, this was easily accomplished. The system was set up to look at a 3 inch by 3 inch square. It could be set up to look at a larger area; however, the smaller the area of interest the better the resolution of the camera. Because it was hypothesized that the velocity flows that would be studied were going to be in the millimeter to centimeter per second range, it seemed logical to keep the resolution as high as possible. From the dye tests, it was known that streaming flow begins shortly before the transducer's focus and extends well past this focus. The camera's view was moved to this location. At this point, the SSP was no longer required and was removed from the tank.

A reference grid target was placed in the tank and the laser was turned on so that the grid could be placed appropriately in the illuminated field for alignment. This target calibrated the field so that the number of meters per pixel was known. To calibrate the camera, the target was moved so that its front face was coincident with the laser sheet. Once this was accomplished, the laser was turned off. The CCD camera was then adjusted slightly to get a sharp focus on the dots. The calculation of resolution was made and inserted into the software program used to measure the velocity of the field.

3.4.2.3 Data acquisition and procedure

Once the system was calibrated and aligned, tracer particles were added to the water to facilitate the PIV process. For this test, TSI brand hollow glass spheres of nominal diameter 10 micron seeded the fluid. An exact measurement of the amount and weight of spheres added was not recorded, but it was estimated to be around 0.1 gram. There is allowable variation from this amount; however, it is important that the system not have too many particles added so that single particle paths could be distinguishable. Dr. O'Halloran recommended the amount used as a rule of thumb. Once the particles were added, a small amount of mixing was required before the distribution of the spheres was uniform.

At this point, the system was isolated with black non-reflecting sheets to aid in proper data collection. Any stray reflected laser light might produce an erroneous data set. Because of this, the highly reflective transducer housing and its necessary holding mechanism (the only apparatus besides the water and tracer particles in the aquarium tank) were completely wrapped with non-reflective tape. The only surface untouched was the Teflon coating of the transducer,

which did not produce damaging reflection. Black sheeting minimized ambient light from windows and doorways, and room lights were turned off. The system was now ready for data acquisition.

The PIV system had an automated data taking process. The key attributes important to modify were laser power and the time between the laser (and data collection) pulses (Δt). The value of laser power brightened the illumination of the hollow glass spheres. It is important to choose a value that is large enough to provide good illumination, but not too large to introduce unnecessary light into the system. As was mentioned earlier, the illumination system is really two lasers; each flash in sequence with a set delay. This delay was also sent to the CCD camera so that as the laser flashes, the camera snaps a picture. The delay needed to be long enough that it would capture the streaming event but short enough so that a tracer particle could be tracked accurately. Based upon an analysis of the PRF of waveforms to be tested (and the expertise of Dr. O'Halloran), a value of 8 ms was chosen.

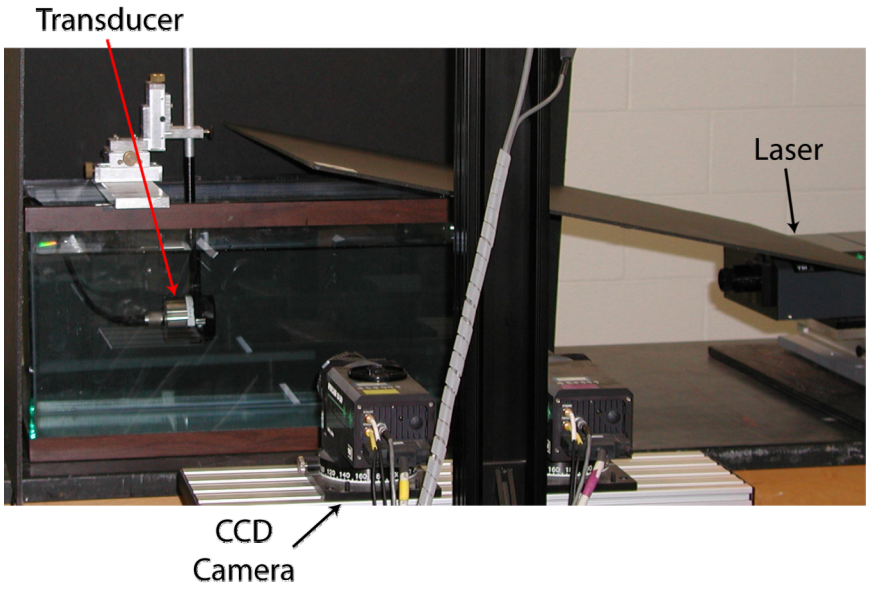

Figure 3-4: The PIV system

The number of data samples taken can also be modified. This number can be large or small because the computer program will process the data and analyze the values to produce the average velocity profile for a data set. Unfortunately, the larger the number of data sets for a particular average, the longer the computer analysis time. After repeated testing and verification of data, it was determined that there was little difference between taking 10 data sets and 50 data sets. The main difference was the amount of background noise (natural water movement) that

could be seen. It was determined that by taking 10 data sets, the main goal of velocity profile could still be reached in far fewer computer hours.

As in the dye tests, data was taken as intensity and duty factor creation were modified. The process for recording a data set was as follows. The output from the function generator was disabled. The appropriate input voltage (to produce the required intensity as measured on the oscilloscope and defined by the k value) was entered into the function generator. The method for duty factor creation was then entered into the function generator. With the newly defined sign wave created, the output of the function generator was enabled. The resulting waveform was confirmed on the oscilloscope. The system was allowed to run for 15 seconds. After 15 seconds, the PIV system was initiated to capture the requested frames. Upon completion of the laser flashing, the output of the function generator was then disabled, and the system was left to rest for 20-30 seconds as the new values were entered into the system and the process was begun again. This allowed for streaming to be properly initiated and be completely dissipated.

Once all the data were taken, the processing of the data began. It is important to note that when using PIV, several instances occurred in which a tracked particle seemed to move farther than it actually did (i.e. in a system with average velocity 5 mm/s, a lone particle moving at 80 cm/s). Because of this, particles that had velocities greater than eight standard deviations from the average were removed from the calculations. When processing was completed, a data file was saved to the computer hard drive.

This data file could be analyzed with a variety of means; however, looking at the data graphically produced the best understanding of the results. With some organizing of the data (through the use of macros and pivot tables) and the use of the contour plot graph in Microsoft Excel, a visualization of the flow could be produced; however, the preferred way to analyze the data was through the use of Tecplot software. This software automatically analyzed a data set and produced flood type contour plots. One of these plots is shown in Figure 3-5. When looking at the Tecplot graphs, note that the values of the X and Y axis are in mm. From the calibration of the PIV system, it is known that the acoustic focus of the transducer was at 22 mm on the X-axis and 37 mm on the Y-axis. Tecplot also automatically generates a legend. For every plot, the velocities range from deep blue (representing the lowest velocity on the chart) to bright red (representing the highest velocity). In Figure 3-5 the velocity data shown in the legend has units

of m/s. Due to software limitations, this legend does not represent the same flow rate/color relationship from graph to graph.

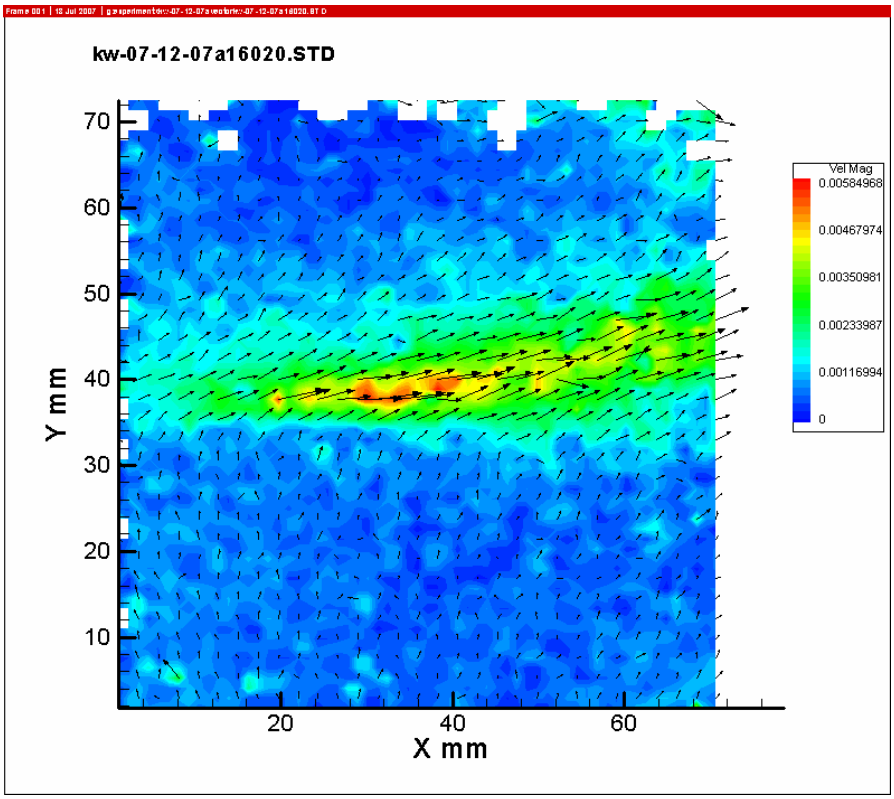

Figure 3-5: The Tecplot flood chart of streaming at a 1% DF, 1035 W/cm^2, 333 Hz PRF, and 35 cycles

3.4.3 PIV data analysis

The data collected from PIV showed that, indeed, there was measurable flow at intensities below those measured in the dye tests. However, at very low intensities the PIV system was not able to find any measurable flow. This usually occurred at low intensities with duty factors produced by a small number of cycles per burst. Figure 3-6 shows the streaming measured at different intensities for a 3% duty factor created using differing number of cycles. The graph shows that at low intensities with few cycles, there was no streaming measured at all. As intensity increased, the velocity increased. The standard deviation was between 0.00096 m/s and 0.00142 m/s. Standard deviation and trend curve is presented on a representative data set (690 cycle data set -- color matched line and points) to eliminate clutter on the graph.

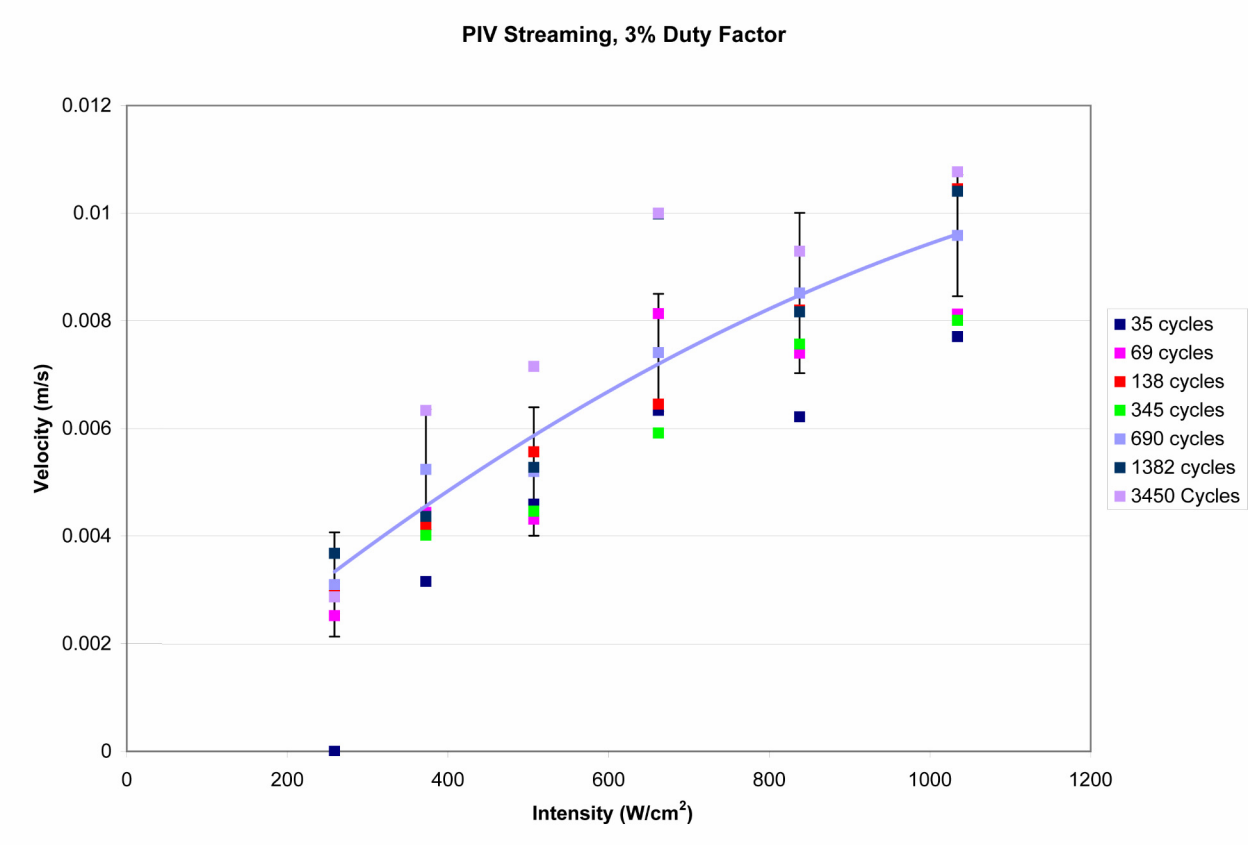

Figure 3-6: Streaming created by a 3% duty factor with different numbers of acoustic cycles

Figure 3-7 shows the streaming produced by different duty factors when the keeping the number of cycles used to create the specific duty factor similar (in this case around 46 +/- 12 cycles per burst.) The figure shows that intensity has a major effect on streaming: the higher the intensity the more measurable the flow. Additionally, as the duty factor increases (meaning that the particular intensity is applied for a longer period), the streaming velocity increases.

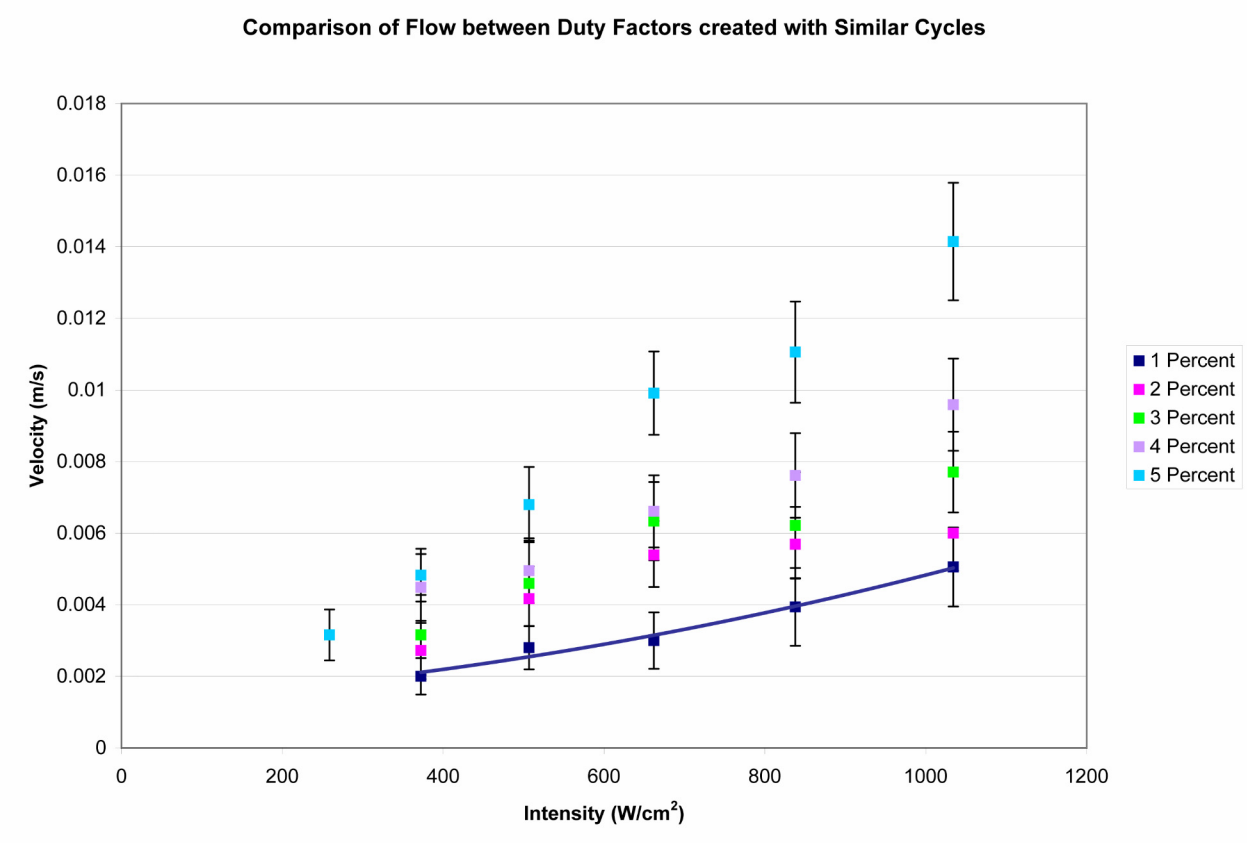

Figure 3-7: Comparison of flow between duty factors created with similar number of cycles

3.4.4 A radiation vs. drag force model of PIV flow

As the literature review indicated, the determination of streaming velocity by analytical means is not a trivial task for pulsed and focused acoustic fields. Complete development and analysis of an all-encompassing model for streaming of a pulsed, focused acoustic field is not the goal in this research; however, a basic model for a PIV system is the goal of this section. Comparison of this model to the actual data will show its validity under certain prescribed conditions. This proposed representation considers a momentum balance of the forces on a "particle of fluid" that is the size of the PIV tracer particle. This analysis will represent the particle as a short cylinder.

In the basic streaming analysis proposed in this section, radiation force will act to propel the particle forward, while Stokes Drag Force will counteract this forward movement to slow the particle down. In this model, the acoustics are driven at low duty factors so while the Stokes Drag force will always be present when movement is occurring, the radiation force will only act as an impulse for the duration that the acoustics are present.

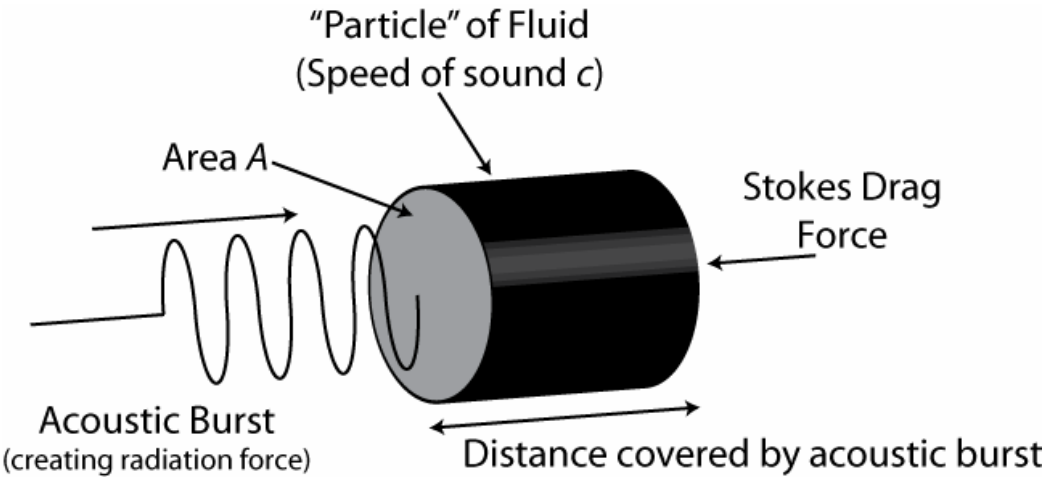

Figure 3-8: The force diagram for a basic streaming analysis

Figure 3-8 illustrates the situation for which the streaming model is developed. This diagram is similar to Figure 2-1, except this particle is one that is moving because of the acoustic radiation force. Resisting the movement is the effect of viscous resistance that the flowing fluid particle will encounter. The size of the fluid particle is based upon the length of the acoustic burst. This model will assume that high-intensity ultrasound will produce a radiation force on the left hand side of the particle of fluid propelling the particle of fluid forward, producing flow. This flow is assumed to be at a relatively slow speed and laminar (therefore having a low Reynolds number, $R_e < 1$). Using these assumptions, the viscous resistance (or drag) is approximately proportional to velocity but opposite in direction. The equation for viscous resistance is:

$$F_d = -b \cdot v \tag{3.9}$$

where F_d is the force created by drag, v is the velocity of the object, and b is a constant that depends upon the properties of the fluid and the dimensions of the object. In the case of a very small object moving slowly through a viscous fluid, Stokes provides an expression for b that is:

$$b = 6\pi\mu r \tag{3.10}$$

where μ is the fluid's dynamic viscosity and r is given as Stokes radius of the particle for very small (molecule sized) objects, but can be considered the effective hydrodynamic radius for particles of larger diameter (but still of small scale).

Applying Newton's Second Law to the fluid particle:

$$F_R - F_d = m\frac{dv}{dt} \tag{3.11}$$

where F_R is the radiation force acting on the particle. Separating the variables and integrating will provide an equation for the final velocity, v_2, based upon the initial velocity, v_1, over the time in which the radiation force acts and is opposed by the viscous drag force, t:

$$v_2 = \frac{F_R}{b} - e^{-\frac{b}{m}t}\left(\frac{F_R}{b} - v_1\right) \tag{3.12}$$

Applying the same logic during the time that an acoustic burst is not applied (defined by the pulse repetition frequency), an equation for the velocity when only viscous drag is affecting the moving fluid particle results:

$$v_2 = v_1 e^{-\frac{b}{m}t} \tag{3.13}$$

By creating a model that applies equation (3.12) during the acoustic burst and equation (3.13) during the off time, an estimate of the streaming velocity can be created.

3.4.4.1 PIV Data compared to radiation force/stokes drag model

By comparing the model to all streaming data, it was determined that it was only applicable to data collected with high values of pulse repetition frequency. When this value decreased, the modeled flow became drag-dominated and produced results that showed no appreciable velocity, which was not the actual case. Importantly, the model did show development time for streaming and a time average flow after that point. In the following pages some representative charts are presented comparing the model to the actual data.

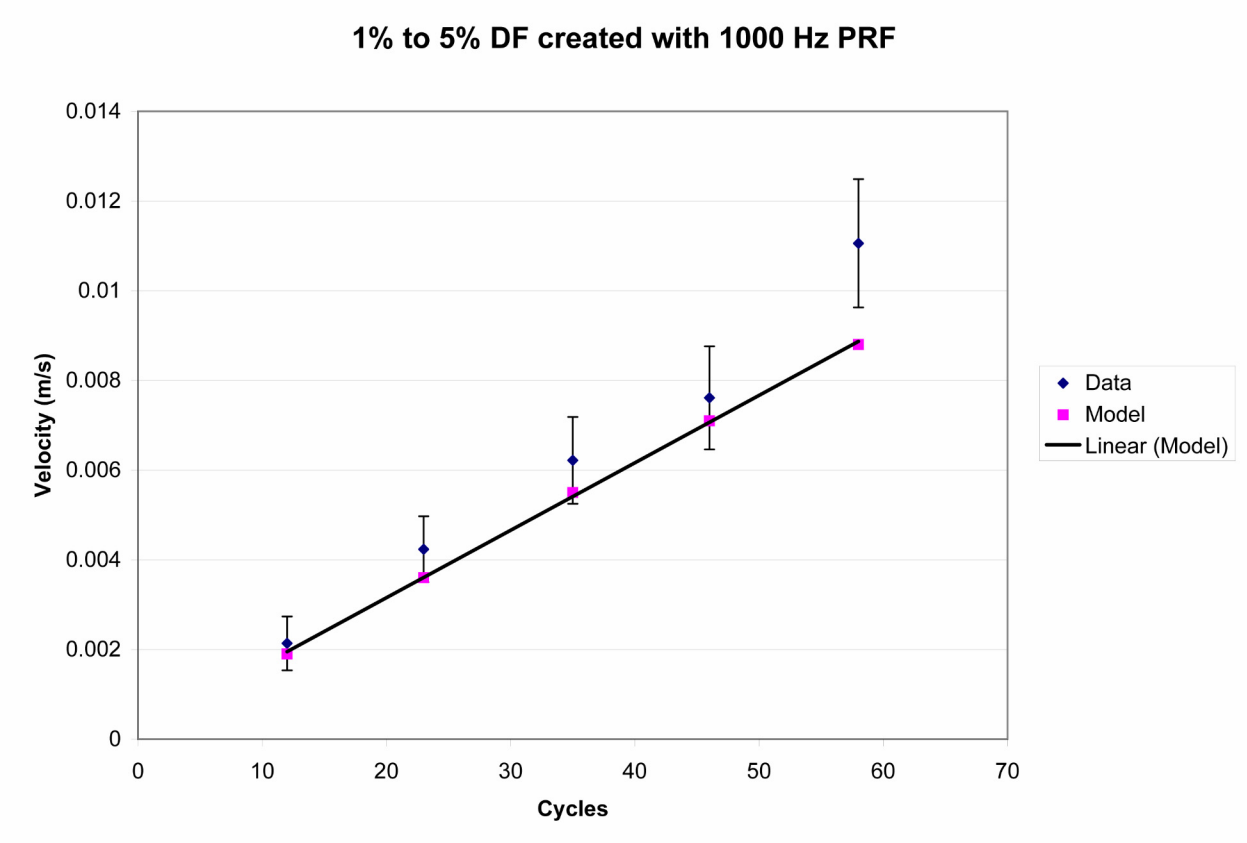

Figure 3-9: Comparison of streaming velocity produced by the model compared to data collected from PIV testing at 372 W/cm^2.

Figure 3-9 shows the comparison of streaming velocity observed to that modeled when the intensity is kept constant but the duty factor is changed. This graph represents duty factors from 1% to 5% using a standard PRF of 1000 Hz. Figure 3-10 illustrates the relationship between measured and modeled values of streaming at a 1% duty factor created at 333 Hz PRF, 35 cycles.

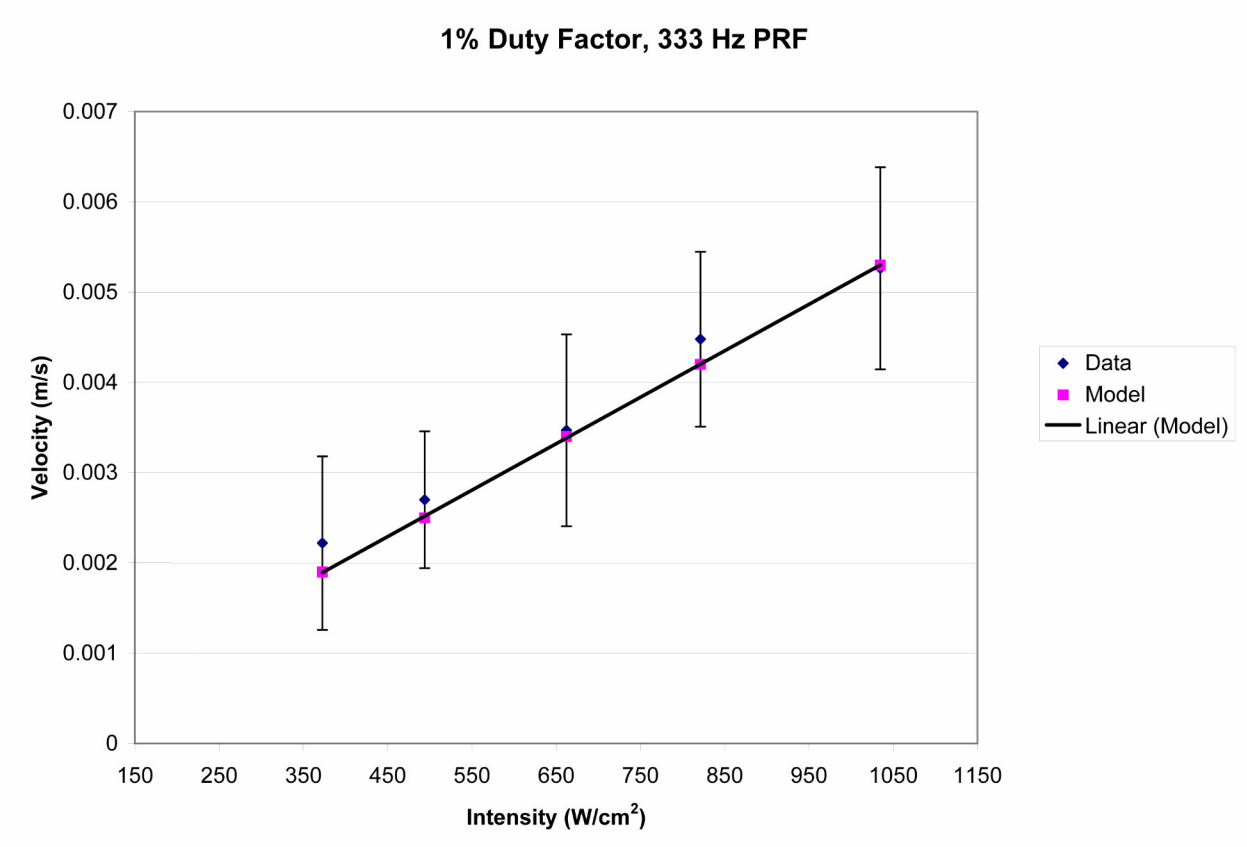

Figure 3-10: Streaming velocity measured vs. modeled values for 1% DF, 333 Hz PRF

3.4.5 Streaming target determination of streaming flow

Another method to determine experimentally the streaming velocity uses the streaming target described in Chapter 2. Recall that a streaming target is made of acoustically transparent Mylar. This target will not deflect due to radiation force but will deflect if it encounters a streaming flow. From a force balance calculation, the value of this streaming force can be determined in terms of deflection. From here, application of a momentum flux analysis to the target will determine the velocity of the incoming stream that would cause the deflection. This calculation bases itself on an analogy to the problem of a jet hitting a vane. Here, consider the target the vane and the streaming the jet hitting that vane. Referencing Figure 3-11 and using a momentum analysis provides:

$$F = \rho A v^2 \tag{3.14}$$

where ρ is the density of the fluid, A is the area of the jet (circular cross section), and u is the velocity of the jet. Rearranging (3.14) gives the velocity of the jet as:

$$v = \sqrt{\frac{F}{\rho A}} \tag{3.15}$$

where the area of the jet is experimentally determined from the measurements collected during the PIV study.

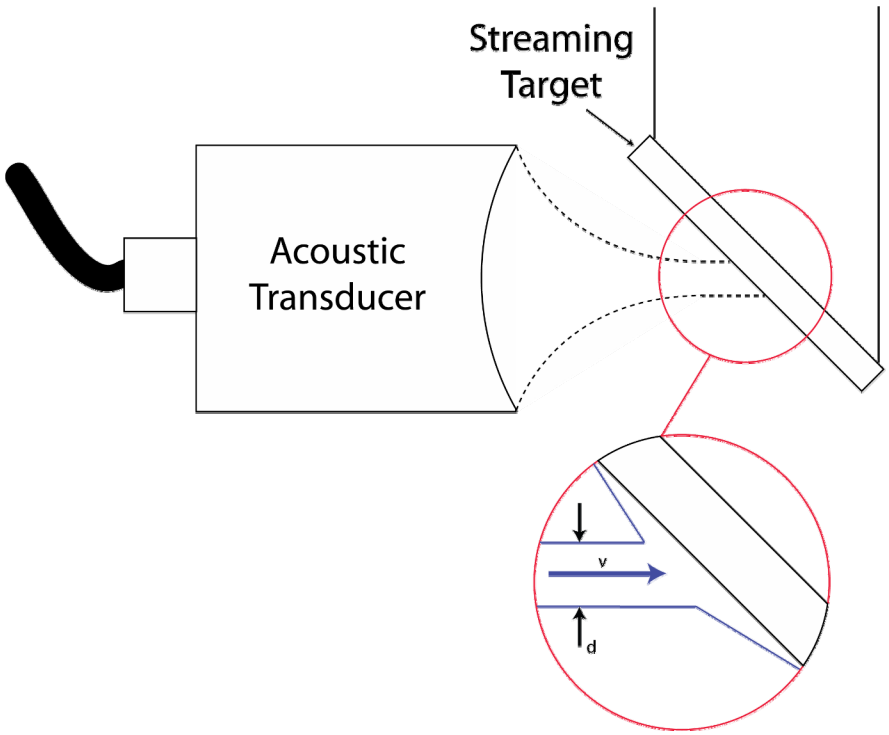

Figure 3-11: Diagram of the streaming target treated as a vane in the path of an acoustic field generated jet.

The streaming target is very sensitive to very small streaming flows; thus, deflection of the target occurred at values below those measured by the PIV system. Interestingly the deflection was higher than the values measured by PIV and lower than those measured by contrast dye. Additionally, the data recorded showed little change in streaming depending on way of creating duty factor. The spread of the data was much closer than that recorded in PIV and dye tests. Figure 3-12 presents the results from this study.

The streaming target intercepts the entire acoustic beam; therefore, it measures the total effect of the ultrasound and does not discriminate based upon the non-uniformity of the acoustic profile. This may explain why the velocities from the streaming target are different than those measured by the dye test or PIV.

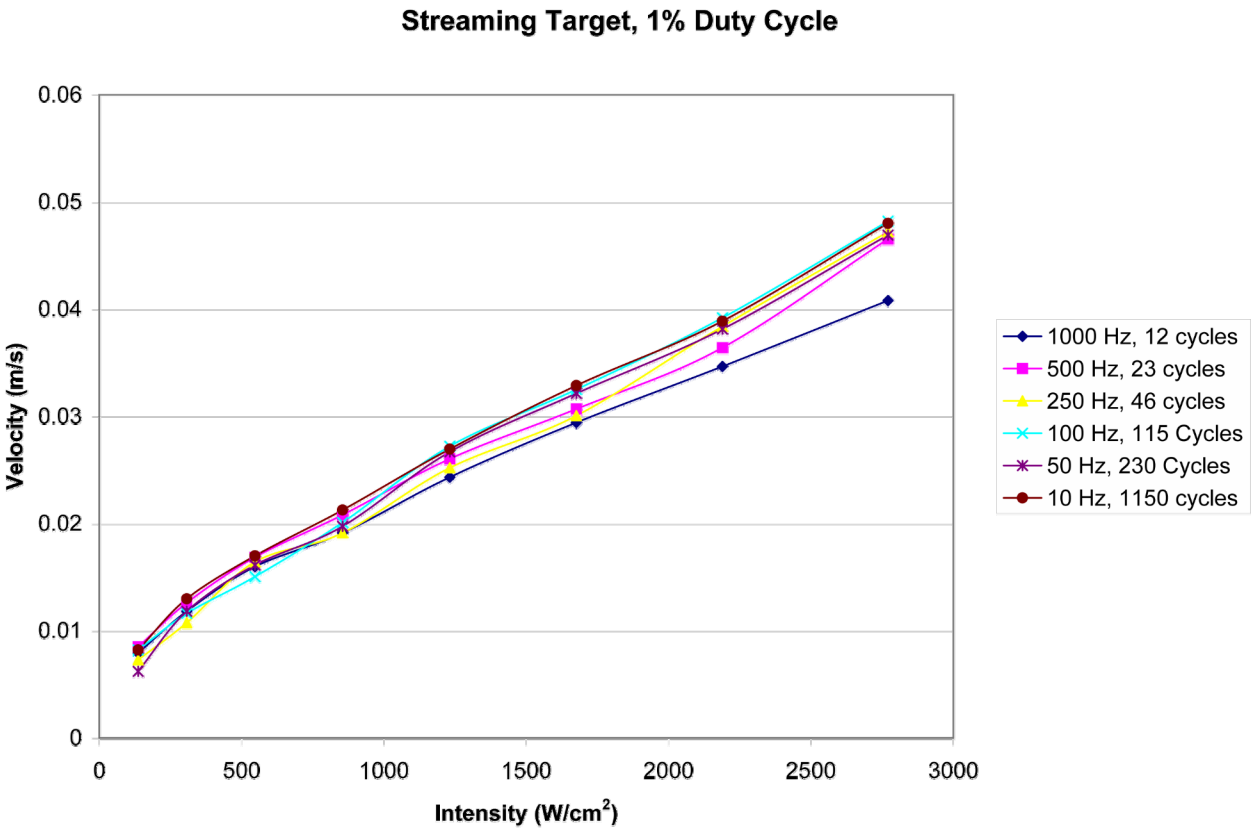

Figure 3-12: Streaming velocity measured by streaming target.

3.5 Summary of acoustic streaming measured by experimental methods

Many researchers have studied acoustic streaming, but most of the analysis has been for plane, continuous waves. Recently, due to the application of high-intensity ultrasound to medical applications, acoustic streaming caused by focused, pulsed sound fields has gained interest. The development of models for such fields has been limited, and when applied, complex.

Experimentally, three methods measured acoustic streaming due to high frequency, pulsed ultrasound. A dye method recognized qualitative movement, but was not precise. To pick up minute moments of the flow, bulk movement had to occur, making it difficult to get accurate readings. A PIV technique allowed for velocity measurement at low intensities not measurable dye, but could not be applied at high intensities due to turbulence created by cavitation. A streaming target method of measuring the flow was tested. This method was very similar to the measurement of the second order radiation force and had direct application to

calibration methods discussed in Chapter 2. Below in Figure 3-13, a comparison of the three methods is presented.

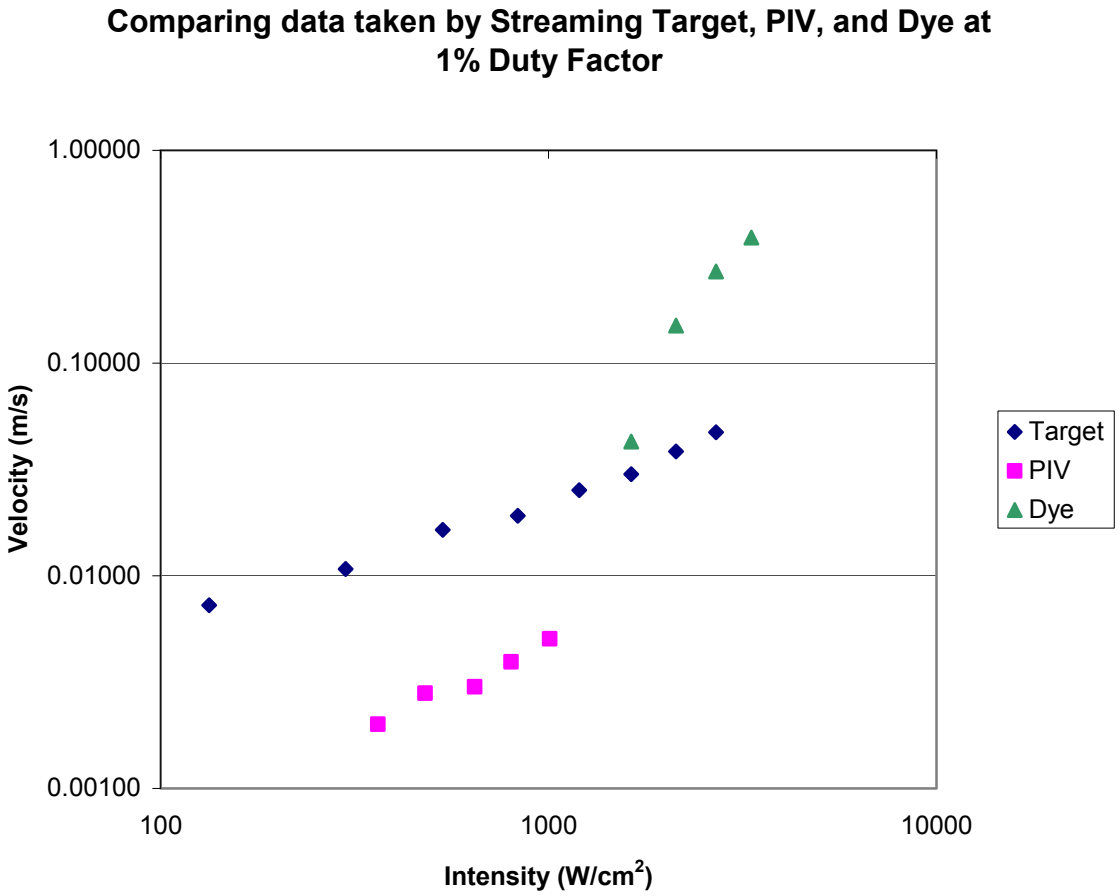

Figure 3-13: Comparing streaming velocities measured by target, PIV, and dye

A basic model for acoustic streaming was proposed in this chapter, and it was found to be applicable in situations where the duty factor was created in such a way that there was a short PRF. Although this model was not universally applicable, it would be sufficient for situations at low intensities with duty factors created with high PRF values to estimate the velocities that would be produced by a high-frequency, pulsed acoustic field.

Acoustic streaming was also experimentally measured using a streaming target. Because the target intercepted the entire ultrasonic beam, a slightly different measure of streaming was produced. Nevertheless, the streaming target measured flow and showed that as intensity increased, streaming velocity did as well.

Acoustic streaming is an important phenomenon in the realm of high-frequency ultrasound. Its existence goes hand in hand with that of acoustic radiation force. In order to more fully understand the results of any experiment with high-frequency fields, the existence of acoustic streaming must be acknowledged.

Chapter 4 - An Estimate of Cavitation Energy

The previous chapters have spoken of effects of the acoustic waveform up to and sometimes including the cavitation threshold. This chapter will focus on the mechanical effects created by high-intensity, focused ultrasound, namely acoustically created cavitation. The goal for this chapter is to provide a method to estimate the energy release of a single cavitation bubble.

A variety of applications use acoustically created microcavitation. Numerous scholarly investigations are presently investigating novel uses of this medium. "Microcavitation Surface Removal" (Wanklyn, 2002) research observed how acoustically created cavitation could be used to remove a variety of surfaces without damaging its underlying substrate. This study showed that cavitation energy, when precisely controlled, could lead to innovative solutions for some complex engineering problems. In Wanklyn's previous study the mechanism researched was cavitation erosion. In this chapter, an application of this knowledge will help to estimate how much energy a cavitation bubble deposits on a surface when it implosively collapses.

4.1 The implosive collapse

To study the energy deposited by a single cavitation bubble this chapter will focus on acoustically created, transient cavitation events. These events occur over a short time scale and implosively collapse, depositing energy to the surroundings. There are two main theories on how the energy deposition occurs: bubble jet, and shock wave. Depending on the situation, both theories may help accurately describe the implosion of a bubble. What follows is a brief introduction.

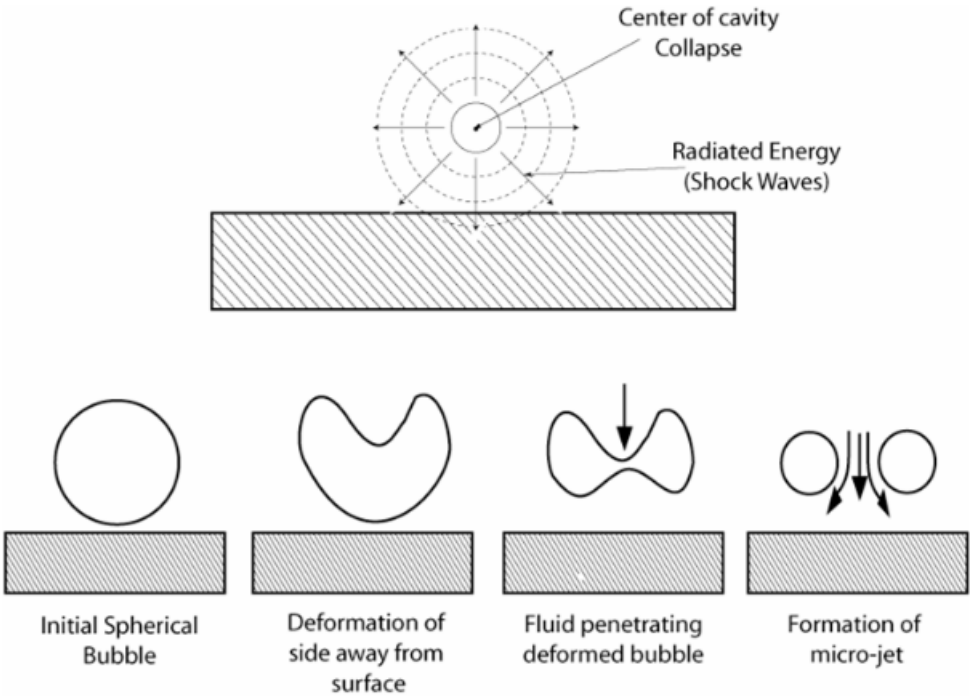

Figure 4-1: Illustration of the different types of collapse mechanisms

Explored in the shock wave/bubble jet debate is the form of the energy that causes cavitation damage. Rayleigh originally approached this question on his initial study of the event. His model showed that a local and very high pressure peak occurred at final collapse (Pereira, Avellan, & Dupont, 1998). Fujikawa and Akamatsu (1980) showed that this pressure peak at collapse created a shock wave in the fluid. This research promoted a shock wave as the cause of cavitation damage.

Other researchers disagree. Their research shows that when a bubble implodes near a solid boundary, that bubble takes on the form of an involuted jet. They propose that this liquid microjet is the root cause for the cavitation erosion.

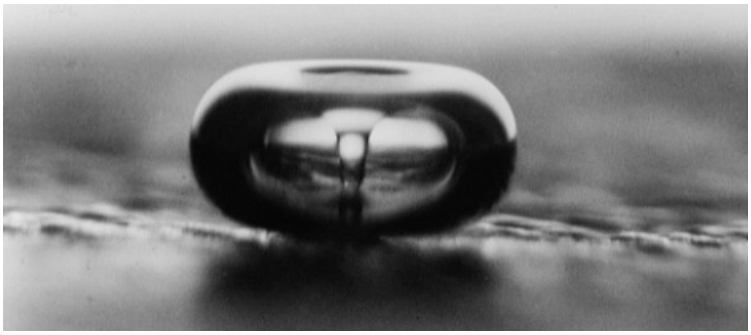

Figure 4-2: Photograph of involuted bubble jet (Photograph by L.A. Crum)

Research is still ongoing in this area; however, it has now become popular opinion that in fact, some combination of these two effects probably influences cavitation erosion, although the shock wave mechanism is gaining influence as the predominant method (Pereira et al., 1998).

4.2 Attempts at energy measurement

Energy measurement of a single cavitation event is a topic that relatively research has been completed. A literature review revealed that what little completed research there is has mostly concentrated on cavitation in the body of a fluid and not on the energy deposition of a cavitating bubble on a surface. The inherent difficulty in measuring the energy of a collapsing cavity is that the cavitation investigated is usually multi-bubble cavitation that is of unknown number, or unknown size distribution, and affected by unknown pressure. It is very difficult to establish a repeatable, controlled, single cavitation event. Overcoming these problems must occur before there can be an acceptable determination of cavitation energy.

In ultrasonic cleaners, the idea of cavitation energy is one of great importance. Cavitation has long been used in ultrasonic tanks to clean many surfaces, especially electronic devices. A problem arises when energy presented to a surface is not enough to clean pristinely the device. Conversely, if too much cleaning energy is present in one location the device may be damaged. One method of measuring cavitation is an indirect method that consists of exposing aluminum foil to the cavitation process and then examining the foil for dents and holes caused by the cavitation. A United States Patent has been given to a device to measure cavitation energy in ultrasonic tanks called an "Apparatus for measuring cavitation energy profiles" (Azar, 2002), but the patent describes a magnitude device rather than a system for measuring actual cavitation energy.

The most significant attempts at measuring cavitation energy come from the world of Sonochemistry. Sonochemistry is the study of how ultrasonics uses high temperatures and pressures of cavitation in chemical systems. Lord Rayleigh described the first model for the collapse of cavities in incompressible liquid and predicted that temperatures of 10,000K and pressures of 10,000 atm could occur during collapse (Suslick, 1990). Experimental values measured by many researchers approach or exceed these values of temperature and pressure. The measurement of temperature occurs when cavitation bubbles start to glow in a phenomenon called sonoluminescence. Analysis of the emitted spectral lines of this glowing light indicates

that the temperature reached inside these bubbles in water can be from 5,000K (Lohse, 2005) to 20,000K (Didenko & Suslick, 2002).

To harness this chemical power of cavitation, however, scientists must first understand, and then control, where the energy is going. To study the energy dissipation during bubble collapse, Suslick and Didenko (2002) first generated a single bubble and drew it to the center of a spherical container where it became trapped in an acoustic field. Driven by ultrasound, the bubble would periodically grow and collapse. With each pulsation, the bubble emitted a flash of light known as single bubble sonoluminescence. While observing the light from a single bubble is as Suslick describes "relatively easy," measuring the high-energy chemical reactions occurring is a challenge. To measure chemical properties, the researchers used sensitive fluorescent detection techniques.

With an acoustic frequency of 52 kHz, Suslick and Didenko calculated that the potential energy of a bubble at its maximum radius (28.6 μm) is 6.4×10^{10} eV. According to the researchers' measurements, less than one millionth of this energy is converted into light. A thousand times more energy goes into chemical reactions, but the largest part of the sonic energy is converted into mechanical energy (Didenko & Suslick, 2002). In researching this method, Didenko and Suslick never directly measured cavitation energy; rather, they measured the amount of OH ions and photons emitted from a bubble and made calculations to quantify the efficiency of sonoluminescence and Sonochemistry based upon a theoretical value.

The Suslick and Didenko study was the most descriptive presented in the literature review. Other resources mentioned the idea of cavitation energy, but provided no experimental measurement. Only in few cases did Sonochemical and sonoluminescence studies determine the energy dissipation of a single bubble. None determined the mechanical energy produced by a single cavitating bubble. The rest of this chapter is devoted to an attempt to find this energy.

4.3 An approach to estimate cavitation energy

There is not a device developed that can be put into a fluid, interact with cavitation, and then produce an energy measurement. This research's aim is to establish an approach to measure the mechanical energy released from a single cavitation event.

Previous research studies completed by the author have allowed the observation that a certain level of intensity will produce acoustically created cavitation that can cause significant

erosion to surfaces. The goal of most past research has been to control where and when these events take place (Wanklyn, 2002). For example, if a xerographic ink-coated sample of paper is presented to a properly initiated acoustic field, cavitation will develop and remove the xerographic ink without damaging the underlying paper substrate (Chandran, 2000). In other research, a properly created acoustic field scanned a silicon wafer. The interaction of the acoustics and the wafer cleaned particles off the substrate, leaving the wafer surface untouched. However, these studies found that scanning the wafer with very high intensity acoustics could pit the wafer surface. These pits look like micron-sized indentations on the wafer surface.

In any case, where cavitation is used to remove particles from or interact with a surface, the result of that interaction should be able to be measured to gather information about what type of energy was needed. The use of the silicon wafer provides an opportunity to complete such a measurement. Silicon wafers are of a known and standard structure. If controlled cavitation pits this type of wafer at a specific, locatable position, measurement of the size of the indentation is possible. Knowing the standard properties of silicon the indentation size can give information about the cavitation event needed to cause such an indentation. From this, an estimation of the mechanical energy released by a cavitation event is possible.

4.3.1 The dynamics of an acoustic bubble

During bubble compression, the potential energy of the bubble converts to mechanical energy. The Rayleigh-Plesset (RP) Equation characterizes the dynamics of bubble motion. While this equation has had many different authors adding specific terms to the equation (Neppiras, Noltlingk, Poritsky) the equation provided is adequate:

$$R\ddot{R} + \frac{3}{2}\dot{R}^2 = \frac{1}{\rho}\left(p_g - P_0 - P(t) - 4\mu\frac{\dot{R}}{R} - \frac{2\sigma}{R} \right) \qquad \textbf{(4.1)}$$

where R is the bubble radius, μ viscosity, p_g the pressure of the gas inside the bubble, P_0 the static pressure, $P(t)$ the pressure of the acoustic wave, and σ the surface tension. This equation has been shown to give reasonable estimates of bubble motion when driven by an acoustic waveform (He, 2004).

This model provides valuable information for the experimental study. It can show given an initial bubble size, how big a cavitation bubble can grow. If the pit caused by cavitation is less than the maximum bubble size modeled by this equation, then it is reasonable to assume that

a single cavitation bubble caused the indentation. This allows the creation of a calculated estimation of single bubble cavitation energy.

4.3.2 Polished silicon wafers

Selected as the standard to measure the energy of a single cavitation event was the single crystal silicon wafer. These wafers are common in the semiconductor industry and have very repeatable physical and chemical properties. This section gives background information to introduce these wafers specifically describing their properties.

Silicon wafers can be fabricated using many techniques, but the one most common is called the Czochralski technique (May & Sze, 2004). This method creates a single crystal of silicon. First, an appropriately oriented seed crystal (e.g. (111)) is placed over melted silicon. The seed is then dipped into the silicon and slowly withdrawn. As withdraw occurs, progressive freezing at the solid/liquid interface creates a large silicon ingot. The diameter of this ingot depends on the pull rate of the seed crystal.

During crystal growth, a known amount of dopant is added to the silicon crystal melt in order to create a desired doping concentration for a grown crystal. Most commonly for silicon, boron and phosphorus are used to create p-type (increases the number of free positive charge carriers) or n-type (increases the number of free negative charge carriers) respectively (May & Sze, 2004).

A grown ingot is now shaped into proper silicon wafers. The ingot is ground into a user-defined diameter (i.e. 200 mm or 300 mm). For wafers 200 mm or smaller, flats are ground into the diameter in order to help mechanized equipment (as well as humans) position and orient the wafer as well as to give the crystal orientation and conductivity type. For wafers larger than 200, mm only a small groove is ground in the ingot for mechanical positioning and orientation purposes. Figure 4-3 shows some common identifying flats.

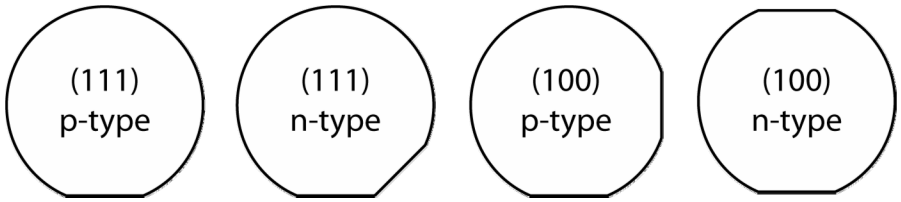

Figure 4-3: Identifying flats of silicon wafers < 200 mm in diameter

Once this process is completed, wafers of determined thickness are sliced from the ingot by a diamond saw. The wafers are then lapped to produce a flatness uniformity of 2 μm with a

mixture of Aluminum Oxide (Al_2O_3) and glycerin (May & Sze). Next, the wafers are polished and are ready for use in semiconductor manufacturing.

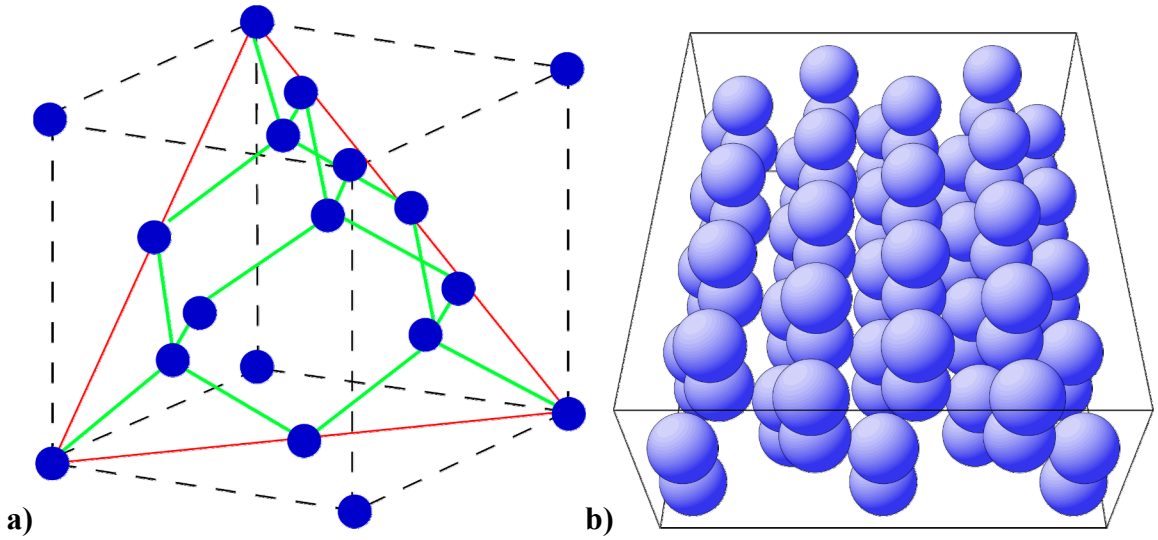

Figure 4-4: The (111) silicon structure a) showing planes in diamond lattice b) showing the atomic structure (with assistance from Surface Explorer)

In this research, 125 mm polished, p-type, (111) silicon wafers 625 μm thick were used. As shown in Figure 4-3, these wafers have a reference flat on their bottom. This type of wafer was selected because crystalline properties will be consistent between two different wafers. This crystalline structure uniformity is crucial in the attempt to determine energy deposition by single bubble cavitation.

4.3.2.1 Miller indices

When describing silicon wafers, the notation (l m n) is used. This denotes planes orthogonal to a direction (l,m,n) (Bullis, 1990). This notation, called Miller indices, provides information about the crystalline structure of the silicon. As illustrated in Figure 4-4 a) the (111) plane is highlighted in red and shows the diamond cubic structure of silicon. Using a web-based program called Surface Explorer[6], the second part of Figure 4-4 shows the atomic packing of (111) silicon.

[6] http://w3.rz-berlin.mpg.de/~rammer/surfexp_prod/SXinput.html

4.4 Experimental apparatus and procedure

To collect experimental data on silicon wafer pitting due to cavitation, a standard setup was established. To summarize, a focused acoustic field was properly aligned with a silicon wafer. Ultrasound of a sufficient intensity was subjected to the wafer so that cavitation pitting would occur. This preset pitting location was scanned by an atomic force microscope (AFM) to determine the amount of silicon removed. Based upon this information, the energy release necessary to create such an indentation was calculated.

4.4.1 The microscope/atomic force microscope

As mentioned, a main part of the testing was to determine the amount of silicon removed from the crystal structure of the wafer. Since these pits were on the micron level in size, optical methods of characterizing the indentation could not be completed. To facilitate the testing, an Atomic Force Microscope (AFM) was used. The AFM provides a small cantilever head with a sharp tip to scan the surface. An AFM can be run in three modes: contact, non-contact, and tapping. A laser references the cantilever and allows the computer to calculate the deviation from normal (Wilson & Bullen, 2006). This data comes together to create a three-dimensional map of the sample's surface. The AFM can be set to have a very fine resolution (nanometer scale) and will be able to determine the geometry of a pit on a silicon wafer caused by a cavitation bubble.

The facilities of Uncopiers, Inc., Manhattan, Kansas were used for the cavitation pit testing. Uncopiers' AFM is a computer-controlled hybrid microscope/AFM. The principle of operation was first to optically locate the area for testing at high magnification (100x) and then use the AFM to scan that area. This was completed with one unit because the turret of the microscope provided both optical and AFM heads. When scanning, the AFM used the tapping method. The speed and size of area looked at by the AFM could be modified to produce higher resolutions and smaller area views.

Since this unit was connected to a computer, it allowed for programming of translation stage movement. This provided better repeatability in locating areas of the silicon wafer subjected to cavitation. In order for this programming to be useful, a standard way of inserting the wafer into the stage of the AFM was developed. The next section describes the apparatus.

4.4.2 The reference indexer apparatus

The challenge with this research was determining where a cavitation event occurs. This was one of the major hurdles addressed. Many different types of setups were used until one of particularly good accuracy was developed. However, even with this apparatus there were challenges that needed to be overcome. This section will describe the development.

4.4.2.1 Hit then find

In the previous section, a quick overview of what was being tried was discussed. A (111), polished, silicon was subjected to cavitation. The area where the cavitation occurred was then visualized, and information about the pitting that the cavitation caused was obtained. The main problem was being able to "hit" an area with cavitation and then subsequently find that exact area. When talking about a 125 mm diameter wafer and a 1.25 mm 3dB focal zone that could produce wafer pitting on a micron scale, the search for cavitation pitting could be the equivalent of looking for a BB pellet on a NCAA football field.

To overcome location difficulties, the silicon wafer was initially marked with a Sharpie marker to locate areas to subject to cavitation. These predetermined locations were then observed by a microscope visioning system to provide pre-test information about the area that would be subjected to cavitation. Once a location spot had been determined, the transducer had to be aimed so that it hit this spot. The transducer was not to interact with the wafer before testing, so inked paper was used to reference where the cavitation would happen. To do this the inked paper was set at the focal distance of the transducer, and cavitation was produced at the threshold of that paper to create a small deinked spot. That deinked spot was visualized by a borescope connected to a television monitor, and a reference noting position was indicated on the monitor. The wafer was then placed in the testing tank in an appropriate holder and positioned properly so that the monitor reference position was placed in the marked area on the wafer. The testing then commenced. When completed, the wafer was taken out of the test tank and again observed under the microscope/AFM to locate any cavitation pitting.

While this method did provide a gross level of location for testing, it provided more variation than was acceptable. One of the main concerns was that the Sharpie marking on the wafer was easily removed (flaked off, dissolved, etc.) upon water immersion. These pieces of marking would settle onto other parts of the wafer, contaminating its surface and the water

sample itself. This contamination would negate any attempts at providing a pristine environment for testing. Additionally, with this method the wafer had to be handled considerably, moved from place to place, reoriented, and replaced. These steps were not ideal for the testing. Another concern was that the optical method for locating the focal spot was not precise. Aiming the transducer, then removing part of the setup to get ready for testing, was not ideal for accurate positioning. Many iterations of this setup were tried until an idea for an entirely different approach was determined.

Apparatus changes provided a non-optical method for repeatably locating a test area. This also allowed the wafer to be handled only once during testing, yet if needed, repeatably located on a standard positioner. It also removed the need to visually mark any aiming spots on the wafer. The goal of these changes was to provide a cleaner, more repeatable setup.

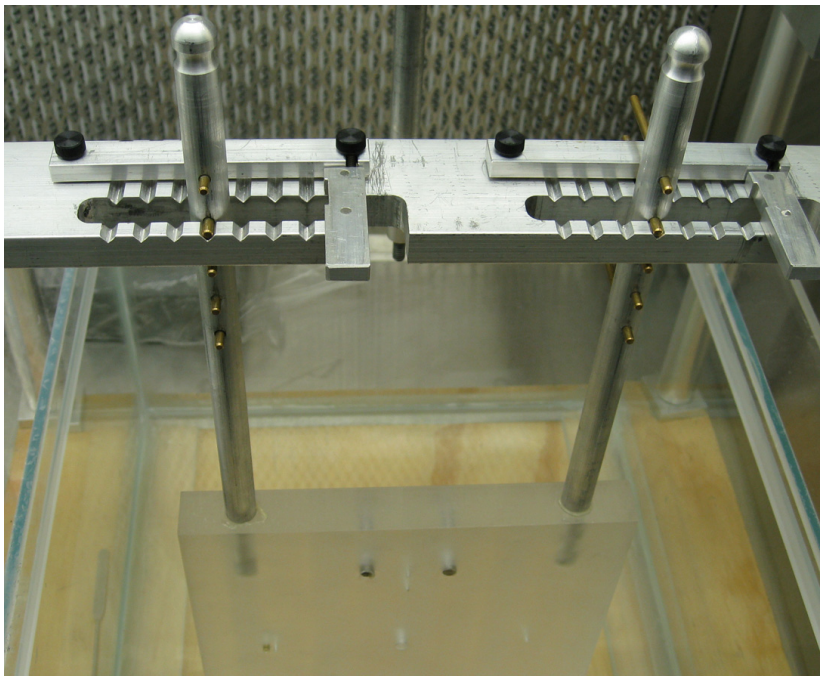

Figure 4-5: Wafer positioning apparatus

To start, a wafer holder was designed and built. This holder could accommodate 125 to 300 mm wafers, allowing them to be placed repeatably and accurately. The wafer holder was designed to be the only moving part in the system. Two referencing plates, one for the microscope/AFM and one for the test tank, were created and rigidly attached to each apparatus. The wafer holder moved between these two plates depending on whether testing or data collection was needed. Once the holder was properly mounted to the referencing plate, it could be secured in place. The referencing plate in the microscope/AFM was attached to the

apparatus' X, Y, Z-axis positioner. In the test tank, the plate was mounted securely with two, quarter inch aluminum bars with locating dowels as shown in Figure 4-5.

As a motorized translation stage was not used in the test tank, a different system was used to position the wafer at different testing sites. This method used locating dowels and corresponding locating slots in an indexer as shown in Figure 4-5. This allowed for the wafer to be moved to 35 consistent locations. Once moved to a different dowel/slot combination the reference plate was secured. Thus, a held wafer could be moved to different places on a standard grid without requiring anything to be modified on the wafer's surface.

Once the wafer holder was moved from the test tank to the Microscope/AFM, the points of testing could be referenced because they were of standard spacing on a grid. This, however, could only be possible if one reference point was consistent between both setups. A calibration technique was needed. To do this, a small 0.065" hole was drilled through the test tank referencing plate and wafer holder to locate the approximate center of the wafer. The dowel/slot system was moved so that it was positioned in the center of its grid. Next, a Sound Signal at a Point (SSP) was placed in the hole and the transducer was aimed so that its maximum acoustic pressure would be coincident with the SSP and thus the center of the hole. Using the location programmable settings of the microscope/AFM, the center of the hole was also located. From this, a single coincident spot was now located on both setups. The rest of the points on the grid could be located.

4.4.3 Testing procedure

The testing procedure was as follows. The test tank was filled with UPW of a 0.05 micron filtration. The wafer holder was then installed on the tank reference plate and a SSP was inserted. Using the oscilloscope to visualize the output voltage of the SSP, the transducer was aimed. Once this was completed, both the transducer and the locating slot indexer were locked into place. The wafer holder was then removed from the tank referencing plate. A wafer was positioned and secured to the holder. The holder was placed in the microscope/AFM, and pre-test screening of the wafer occurred to verify that there was no pre-existing pitting at the testing sites. When completed, the holder was removed and placed on the tank referencing plate. The dowel and slot locater were set so that the transducer was aimed at the center point in the grid. Testing then commenced, first with the center spot, subjecting it to a considerable amount of

cavitation to produce significant pitting so that the researcher could be certain when using the microscope that the center point had proper alignment in the grid. Once the center point was completed, the other 34 points were subjected to cavitation using the attributes selected for testing. The wafer holder was then removed from the tank and placed on the microscope/AFM for pitting investigation.

It is important to note that particles attaching to the wafer were of significant interest in this study. When searching for cavitation pitting, the initial optical difference between a small particle on the wafer and a cavitation pit is difficult to distinguish. Therefore, in this study pristine silicon wafers were used. Upon inserting these wafers in the water, particles adhere to the surface because the free surface of the water was a significant source of particles. Therefore, the entire wafer was immersed in order to avoid creating a significant water line mark on the wafer. When removing from the water, the wafer holder was taken out in one smooth motion to create sheeting action by the water off the surface. Any water remaining on the surface would create spotting. These spots do not derail a test, but they make the job of the researcher searching for a pit more difficult because the pits have to be distinguished from water spots and small particles.

4.4.3.1 Pertinent acoustic variables

Assuring that cavitation occurred at the surface of the wafer during these tests was very important. The challenge was to create sufficient cavitation, not simply a single event coincident with the cavitation threshold. Even though the development of the placing apparatus allowed the location of the pitting to be known, the probability of a single event creating locatable and measurable pitting is low. To solve this problem, cloud cavitation was created. Cloud cavitation occurred in plumes approximately the diameter of the acoustic beam width. Creating this type of cavitation assured that a large number of possible pit-initiating bubbles were produced. This increased the likelihood of creating a locatable indentation on the silicon wafer surface. The creation of this amount of cavitation does not derail the study of single bubble energy. The RP equation analysis shows that the size of pitting can help recognize that caused by a single bubble.

As mentioned, the likelihood of a single bubble creating a locatable, pit on the wafer was low. Similarly, the occurrence of a pit with one cycle of cloud cavitation was also low. Therefore, in experimental testing different amounts of cavitation (from 5-15 acoustic bursts) were applied to the surface. These bursts were counted by creating a 1 Hz pulse repetition

frequency. Thus, an acoustic burst would occur each second. It is assumed that one burst creates one cavitation bubble. Therefore, from the knowledge of how many bursts are applied to the wafer and the number of cavitation bubbles per burst, the number of cavitation events imparted on the surface could be determined.

4.5 Energy estimates

Two calculations will be provided to help estimate the energy of a single cavitation bubble. The first calculation will provide an estimate of the energy available in a fully grown bubble before implosion. The second calculation considers the amount of energy needed to remove each individual silicon atom from the volume of the pit created by cavitation. Dividing this energy by the assumed number of bubbles interacting with the surface gives an estimation of the mechanical energy required by single cavitation bubble. Comparison of these two calculated energy values will provide the estimated percentage of available cavitation energy converted to mechanical energy.

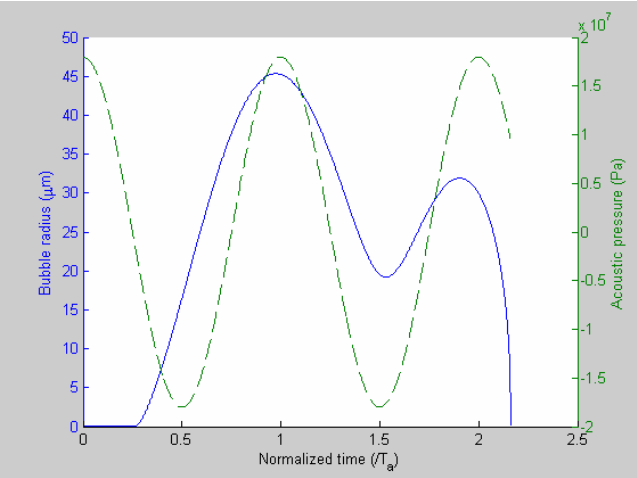

Figure 4-6: The response of a bubble to a 1.15 MHz waveform

4.5.1 Theoretical energy of a bubble

The RP equation aided in finding the total amount of energy available in a cavitation bubble. The model required input of the pressure created by the acoustic transducer, and the initial bubble size expected for cavitation growth. Using this data, the model provided the maximum radius the bubble would attain and how many cycles this bubble would last. In this experimentation, a set pressure was used to grow a bubble from an initial bubble size. This bubble size was not known, nor was it able to be measured experimentally. When running the

model for a range of initial bubble sizes a standard maximum size of 45 micron radius was determined, lasting 2 acoustic cycles. (See Figure 4-6)

With this information a measure of the amount of energy available in this bubble can be made by (Leighton, 1994):

$$Bubble\ Energy = P\not{V} \tag{4.2}$$

where P is the acoustic pressure applied and $\not{V}$ is the maximum volume of the bubble. The RP equation shows that this bubble energy will be applied as the bubble collapses every two acoustic cycles.

4.5.2 Silicon lattice energy

After subjecting the silicon surface to cavitation, the site was investigated with the microscope to find a created pit, and that pit was measured by the AFM. Figure 4-7 shows a typical AFM scan. It is important to note that the size of the pit is much smaller than the RP modeled size of the cavitation bubble, so the assumption of single bubble cavitation creating this pit is acceptable. The AFM collects data in three dimensions providing a 2-D plane view of the pit that can be selected appropriately to view appropriate 2-D cross sections. These maps allowed measurement of pit dimensions and showed that pits often were symmetrical in geometry. Using these dimensions, the volume of the pit was calculated.

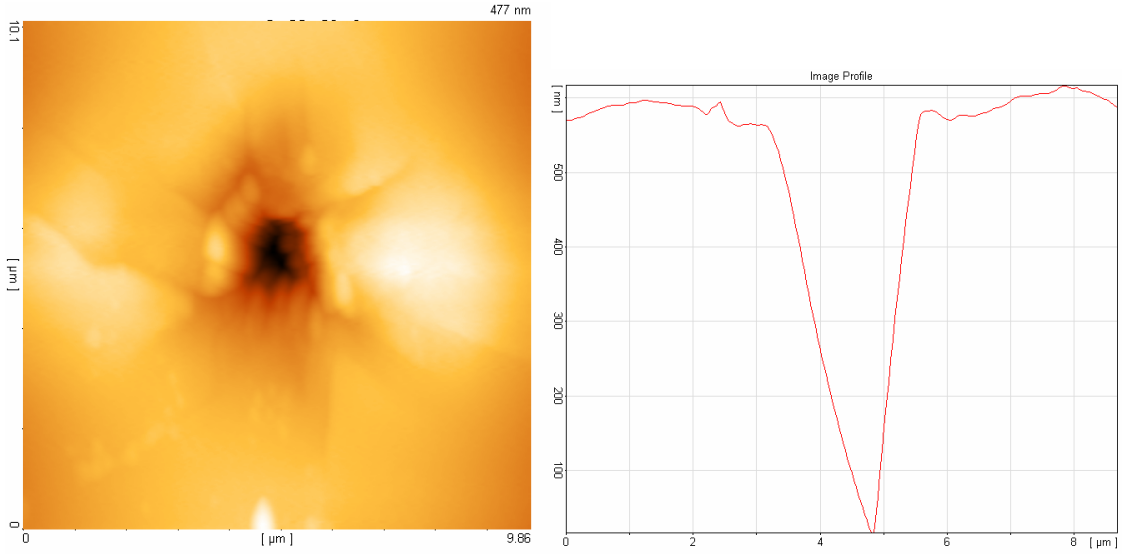

Figure 4-7: An AFM scan of a typical pit created by cavitation and its associated depth profile

Next, the number of silicon atoms that packed that volume was calculated. The atomic radius of silicon is 114 pm and the lattice spacing is 0.5430710 nm. Since (111) silicon is in a diamond lattice, the planes are not uniformly spaced. Each pair of closely spaced planes is separated from the adjacent pairs by a much larger distance. The distance between adjacent planes is 0.3135 nm and the distance between closely spaced planes is 0.0784 nm (Bullis, 1990). Bulatov and Cai (2006) provide that the number density silicon with a diamond crystalline structure is 0.05 atoms/cubic angstrom.

Using the standard information about the silicon lattice and the AFM measured size of the pit; the number of atoms of silicon removed in a created pit was calculated. In order to determine the energy needed to release this silicon, the binding, (or lattice) energy of each atom must be found. This value cannot be directly measured so a reference theoretical model was used to find that this energy was 4.6 eV/atom (Bulatov & Cai, 2006). The model used in this determination cavitation energy assumes that every silicon atom is removed independently of each other. This provides the upper limit of possible cavitation energy provided to the wafer surface. So, by multiplying the number of atoms removed by the lattice energy an estimate of the amount of cavitation energy needed to create the pit is determined.

The assumption is made that the calculated cavitation energy was not applied all at once, but rather in sum by each cavitation bubble as it imploded on the surface. Therefore, to find the mechanical energy deposited by the release of a single bubble, the available lattice energy was divided by the number of bubbles that could interact with the site based upon number of acoustic cycles interacting with the surface. This calculation provides an estimate of the single bubble mechanical energy.

4.5.3 Cavitation efficiency

To summarize the data, Table 4-1 presents representative calculations from the data collected. In the first column, the number of acoustic bursts were applied to the wafer surface. Allowing for the ringing in and out of the transducer, each burst was assumed to be able to produce one cavitation event. In the second and third columns the geometric measurements of the pit are provided. These measurements come from the AFM scan. With this information, the volume of the pit is known. The fourth column provides the energy needed to individually remove every silicon atom from the calculated volume from a lattice energy perspective. The

fifth column provides the energy available from a single bubble as per equation (4.2). Column six takes the calculated lattice energy and divides it by the number of cavitation bubbles possible at the site to determine the energy release by a single cavitation bubble. The final column compares this measured single bubble energy to the theoretical estimation made by equation (4.2). By this estimation only a small fraction of the total bubble energy was converted to mechanical energy, leaving most of the energy to leave the bubble through other mechanisms or to not be directly coupled to the wafer surface.

Number of acoustic bursts	*Diameter of pit (nm)*	*Depth of pit (nm)*	*Lattice Energy* (eV)*	*Single Bubble Energy (eV)*	*Measured Single Bubble Energy† (eV)*	*% Mechanical Energy Deposited on Wafer*
5	2690	300	2.01E+11	4.35E+13	4.02E+10	0.093%
5	2410	325	1.44E+11	4.35E+13	2.88E+10	0.066%
5	2350	450	1.91E+11	4.35E+13	3.82E+10	0.088%
10	2370	600	2.58E+11	4.35E+13	2.58E+10	0.059%
10	2750	550	3.18E+11	4.35E+13	3.18E+10	0.073%
10	2380	700	3.04E+11	4.35E+13	3.04E+10	0.070%
15	3090	650	4.76E+11	4.35E+13	3.17E+10	0.073%
15	3130	600	4.51E+11	4.35E+13	3.01E+10	0.069%

* 4.6eV by silicon atoms removed in pit
† - Lattice energy/Number of cavitation bubbles

Table 4-1: Typical energy estimates for low number of acoustic bursts.

4.6 Summary and future work

The measurement of the energy imparted on a surface by a cavitation event is one not completed in the past due to the limitations of measuring such energy. Past research has focused on the area of Sonochemistry and sonoluminescence to determine any information about a cavitation event. To investigate this problem and propose a solution, an estimation of the amount of cavitation energy deposited on a surface using standard single crystal silicon wafers. By creating, locating, and measuring the pit caused by cavitation on such a wafer, the energy required to create such pitting can be calculated. Experimental measurements provide an estimation of the amount of energy deposited during a single cavitation event.

Future research is necessary to provide a more complete look at the use of silicon wafer pitting as a standard to measure the energy of cavitation events. The testing of different types of cavitation, potentially that of single bubbles alone rather than single bubbles in clouds, would be

important to study if such cavitation could be reliably created. Additionally, analysis of the removed silicon would be very interesting in order to determine if the assumption of single atom removal is applicable or not. This research used an atomic force microscope due to its availability; however, other microscopy methods might provide insight and verification of the geometry of the cavitation-generated pit.

Cavitation is a fascinating phenomenon. It can be considered good or evil depending on the perspective. The facts are clear; cavitation can deposit huge energy densities. Cavitation can damage sensitive parts, but if properly controlled, can provide great benefit. Whatever the case, the introduction of a technique to measuring the pit created by a single cavitation bubble on a silicon wafer does present a new procedure to estimate the energy deposition of acoustically created microcavitation.

Bibliography

AIUM/NEMA. (1992). *Standard for real-time display of thermal and mechanical indices of diagnostic ultrasound equipment.* Rockville, MD: National Manufacturer's Association.

Apfel, R. E. (1972). The tensile strength of liquids. *Scientific American, 227*, 10.

Azar, L. (2002). United States of America Patent No. 6450184. U. S. o. America.

Bulatov, V., & Cai, W. (2006). *Computer Simulations of Dislocations*: Oxford University Press.

Bullis, W. M. (1990). Silicon Material Properties. In W. C. O'Mara, R. B. Herring & L. B. Hunt (Eds.), *Handbook of Semiconductor Silicon Technology*: William Andrew Publishing.

Chandran, J. B. (2000). *Microcavitation studies of surface erosion.* Unpublished Dissertation, Kansas State University, Manhattan, Kansas.

Didenko, Y. T., & Suslick, K. S. (2002). The energy efficiency of formation of photons, radicals and ions during single-bubble cavitation. *Nature, 418*, 394-397.

Drain, L. E. (1980). *The Laser Doppler Technique*. New York: John Wiley and Sons.

Duck, F. A. (1998). Radiation Pressure and Acoustic Streaming. In F. A. Duck, A. C. Baker & H. C. Starritt (Eds.), *Ultrasound in Medicine*. Philadelphia: Institute of Physics Publishing.

Dymling, S. O., Persson, H. W., Hertz, T. G., & Lindstrom, K. (1991). A new ultrasonic method for fluid property measurements. *Ultrasound in Medicine & Biology, 17*(5), 497-500.

Eckart, C. (1948). Vortices and streams caused by sound waves. *Physical Review, 73*, 68-76.

Fox, F. E., & Herzfeld, K. F. (1950). On the forces producing the ultrasonic wind. *Physical Review, 78*, 156-157.

Fujikawa, S., & Akamatsu, T. (1980). Effects of the non-equilibrium condensation of vapour on the pressure wave produced by the collapse of a bubble in a liquid. *Journal of Fluid Mechanics, 97*, 31.

Greenway, M. J. (1999). *An imaging system for the observation of micro-cavitation.* Unpublished Master's Thesis, Kansas State University, Manhattan, Kansas.

He, B. (2004). *An investigation of cavitation thresholds.* Unpublished Dissertation, Kansas State University, Manhattan, Kansas.

Jackson, J. D. (1995). Osborne Reynolds: Scientist, Engineer and Pioneer. *Proceedings: Mathematical and Physical Sciences, 451*(1941), 49-86.

Kamakura, T., Matsuda, K., Kumamoto, Y., & Breazeale, M. (1995). Acoustic streaming induced in focused Gaussian beams. *Journal of the Acoustical Society of America, 97*, 2740-2746.

Leighton, T. G. (1994). *The Acoustic Bubble*. San Diego, California: Academic Press, Inc.

Lohse, D. (2005). Sonoluminescence: Cavitation hots up. *Nature, 434*, 33-34.

Madanshetty, S. I., & Chandran, J. B. (2005). Know thy sound field. *Acoustic Research Letters Online (ARLO), 6*(3), 169-174.

Markham, J. J. (1952). Second-order acoustic fields: Streaming with viscosity and relaxation. *Physical Review, 86*, 497-502.

May, G. S., & Sze, S. M. (2004). *Fundamentals of Semiconductor Fabrication*. United States of America: John Wiley & Sons, Inc.

Medwin, M. (1954). An acoustic streaming experiment in gases. *Journal of the Acoustical Society of America, 26*, 332-341.

Merzkirch, W. (1987). *Flow Visualization*. London: Academic Press.

Nowicki, A., Secomski, W., & Wojcik, J. (1997). Acoustic Streaming: comparison of low amplitude linear model with streaming velocities measured by 32-MHz Doppler. *UItrasound in Medicine and Biology, 23*, 783-791.

Nyborg, W. L. M. (1965). *Acoustic Streaming* (Vol. 2b). New York: Academic Press.

O'Halloran, S. (2002). *Users Manual for Particle Imagining Velocimetry System, Complex Fluid Flows Laboratory, Kansas State University*.Unpublished manuscript.

Pereira, F., Avellan, F., & Dupont, P. (1998). Prediction of cavitation erosion - an energy approach. *Journal of Fluids Engineering, 120*, 9.

Piercy, J. E., & Lamb, J. (1954). Acoustic streaming in liquids. *Proceeding of the Royal Society, A229*, 43-50.

Preston, R. C. (1991). *Output measurements for medical ultrasound*. New York: Springer-Verlag.

Rayleigh, L. (1884). On the circulation of air observed in Kundt's Tubes, and on some allied acoustical problems. *Philosophical Transactions from the Royal Society of London, 175*(1), 1-21.

Rooney, J. (1988). Other Nonlinear Acoustic Phenomena. In K. S. Suslick (Ed.), *Ultrasound: Its Chemical, Physical, and Biological Effects*. New York: VCH Publishers.

Starritt, H. C. (1990). *Streaming induced by high amplitude acoustic pulses and its implications.* Unpublished Dissertation, University of Bath.

Starritt, H. C., Duck, F. A., & Humphrey, V. F. (1989). An experimental investigation of streaming in pulsed diagnostic ultrasound beams. *Ultrasound in Medicine & Biology, 15*(4), 363-373.

Suslick, K. S. (1990). Sonochemistry. *Science, 247*(4949), 1439-1445.

Thornycroft, J., & Barnaby, S. W. (1895). Torpedo Boat Destroyers. *Minutes of proceedings of the Institution of Civil Engineers, 122*(67), 50-107.

Tjotta, S. (1959). On some non-linear effects in sound fields, with special emphasis on the generation of vorticity and the formation of streaming patterns. *Archiv for Mathematic og Naturvidenskab, 55*, 1-68.

Torr, G. R. (1984). The acoustic radiation force. *American Journal of Physics, 52*(5), 402-409.

Trahey, G., Palmeri, M., Bentley, R., & Nightingale, K. (2004). Acoustic radiation force impulse imaging of the mechanical properties of arteries and results. *Ultrasound in Medicine & Biology, 30*(9), 1163-1171.

Vinogradov, A., & Schwarz, M. (2002). *Piezoelectricity in Polymers* (Vol. 2): John Wiley and Sons.

Wanklyn, K. (2002). *A study of microcavitation at surfaces.* Unpublished Master's Thesis Kansas State University, Manhattan, Kansas.

Wanklyn, K. (2006). An overview of acoustic cavitation threshold. Kansas State Univeristy.

Williamson, P. (2008). Discussion of filter rating procedure for the microelectronics industry by Entegris, Inc. Product Support, Phone Conversation, June 11, 2008.

Wilson, R., & Bullen, H. (2006). Introduction to Scanning Probe Microscopy (SPM) [Electronic Version]. Retrieved May 3, 2008 from http://asdlib.org/onlineArticles/ecourseware/Bullen/SPMModule_BasicTheoryAFM.pdf.

Wu, J., & Du, G. (1993). Acoustic streaming generated by a focused Gaussian beam and finite amplitude tonebursts. *Ultrasound in Medicine & Biology, 19*(2), 167-176.

Zarembo, L. K. (1971). Acoustic Streaming (J. S. Wood, Trans.). In L. D. Rozenberg (Ed.), *High Intensity Ultrasonic Fields*. New York: Plenum Press.